

Feasibility of double electrochemical flow cell for high current density conversion of heat to electricity

Plazanić, Marko

Master's thesis / Diplomski rad

2017

Degree Grantor / Ustanova koja je dodijelila akademski / stručni stupanj: **University of Zagreb, Faculty of Chemical Engineering and Technology / Sveučilište u Zagrebu, Fakultet kemijskog inženjerstva i tehnologije**

Permanent link / Trajna poveznica: <https://urn.nsk.hr/urn:nbn:hr:149:687784>

Rights / Prava: [In copyright](#) / [Zaštićeno autorskim pravom.](#)

Download date / Datum preuzimanja: **2024-04-25**



Repository / Repozitorij:

[Repository of Faculty of Chemical Engineering and Technology University of Zagreb](#)



SVEUČILIŠTE U ZAGREBU
FAKULTET KEMIJSKOG INŽENJERSTVA I TEHNOLOGIJE
SVEUČILIŠNI DIPLOMSKI STUDIJ

Marko Plazanić

DIPLOMSKI RAD

Zagreb, rujan 2017.

SVEUČILIŠTE U ZAGREBU
FAKULTET KEMIJSKOG INŽENJERSTVA I TEHNOLOGIJE
SVEUČILIŠNI DIPLOMSKI STUDIJ

Marko Plazanić

Izvodljivost dvostruko-protočne elektrokemijske ćelije za pretvorbu topline u električnu energiju kod visokih gustoća struje

DIPLOMSKI RAD

Voditelj rada: prof. dr. sc. Zoran Mandić

Članovi ispitnog povjerenstva:

prof. dr. sc. Zoran Mandić

prof. dr. sc. Marko Rogošić

doc. dr. sc. Domagoj Vrsaljko

Zagreb, rujan 2017.

UNIVERSITY OF ZAGREB
FACULTY OF CHEMICAL ENGINEERING AND TECHNOLOGY
GRADUATE STUDIES

Marko Plazanić

MASTER THESIS

Zagreb, rujan 2017.

UNIVERSITY OF ZAGREB
FACULTY OF CHEMICAL ENGINEERING AND TECHNOLOGY
GRADUATE STUDIES

Marko Plazanić

Feasibility of double electrochemical flow cell for high current density conversion of heat to electricity

MASTER THESIS

Supervisor: prof. dr. sc. Zoran Mandić

Members of the defence committee:

prof. dr. sc. Zoran Mandić
prof. dr. sc. Marko Rogošić
doc. dr. sc. Domagoj Vrsaljko

Zagreb, september 2017.

I'd like to thank everyone at Aarhus University for the great time and support that was given to me during my stay there.

I would especially like to thank David Ø-M., without whom this work could not have been accomplished.

To Anders Bentzen for having me stay at AU, and to his great optimism that never seems to fade.

To prof. Ante Jukić, for taking time to selflessly help a student.

To prof. Zoran Mandić, whose guidance and teachings led me to this work and overall interest in this field.

I am very thankful to Emil Dražević, above all, for the friendship and good time we had together.

I would also like to thank my dear friends at Zagreb University: Filip, Predrag, Tea and Tin for all the support they have not given me.

And to all the other staff at Zagreb University for sharing good times with me.

Također se zahvaljujem majci i ocu na bezuvjetnoj ljubavi s kojom ne posustaju.

Y al final, doy mis gracias a Usted.

Sažetak

Ispitana je izvedivost dvostrukog elektrokemijskog protočnog članka za pretvorbu toplinske u električnu energiju, odnosno da li se mogu upotrijebiti kao toplinski motor.

U ovom radu se pokušava iskoristiti svojstvo redoks tvari gdje se potencijal neke redoks aktivne tvari mijenja drukčije s temperaturom. U teoriji, ako dva članka s istim redoks parovima rade na različitim temperaturama, zbog toga što im potencijal različito ovisi o temperaturi, generira se razlika potencijala iz koje se može izvući struja i prema tome snaga koje se može pretvoriti u rad. U tom smislu, konstruiran je toplinski motor s dvostruko-protočnim elektrokemijskim člancima. Kako bi se procijenili najprikladniji redoks parovi za toplinski motor, temperaturni koeficijenti, odnosno Seebeck koeficijenti, različitih redoks parova su određivani metodom cikličke voltametrije (CV).

Provedena su osnovna mjerenja kako bi se odredile termodinamičke i kinetičke karakteristike ispitivanih protočnih članaka, tj. toplinskog motora. Ispitan je utjecaj različitih vrijednosti razlika temperatura (ΔT) i stupnja napunjenosti (*states-of-charge* (SOC)) na karakteristike pretvornika s dvostruko-protočnim elektrokemijskim ćelijama. Provedena su mjerenja na potencijalu otvorenog kruga (OCV) te su određivane polarizacijske krivulje.

Ostvarene su gustoće struje od 2 mA/cm^2 kroz pretvorbu toplinske u električnu energiju, te mjerenja ukazuju da je koncept izvediv uz prethodnu optimizaciju članaka i bolje razumijevanje parametara koji utječu na razliku potencijala.

Ključne riječi: elektrokemijski protočni članak, toplinski motor, Seebeck koeficijent, CV, SOC, polarizacijska krivulja, gustoće struje

Abstract

Feasibility of a double electrochemical flow cell for conversion of heat to electricity has been examined, i.e. the research question was if this system could be used as a heat engine.

Redox species have temperature dependent redox potentials, and this dependence is different for different redox species. In theory if one has two different electrochemical cells at two different temperatures, with same redox species on the positive and the negative side, there should be a difference in potentials between two cells from which one could extract current and thus power that can be used for work. In this sense, two cell electrochemical heat engine has been constructed. In order to assess which redox pairs would be the most suitable for the heat engine, temperature dependent redox potentials, i.e. Seebeck coefficients, of different redox pairs were measured by cyclic voltammetry (CV).

Basic measurements regarding batteries thermodynamics and its kinetics were conducted. Various sets of temperature differences (ΔT) and states-of-charge (*SOC*) values on the characteristics of two cell electrochemical heat engine were examined with battery tester. Measurements at open circuit voltages (*OCVs*) were conducted and polarisation curves were determined.

Current densities of 2 mA/cm² were achieved through conversion of heat to electricity and the measurements indicate electrochemical heat engine is feasible, however, it is necessary to further optimize the setup and the measurement procedure.

Keywords: flow cell, heat engine, Seebeck coefficient, CV, *SOC*, polarisation curve, current density

Table of Contents

1	Introduction	1
2	Theory	3
2.1	Flow batteries in general.....	3
2.2	Cell potential of a flow battery	5
2.3	Heat engines	6
2.3.1	General thermodynamics on heat engines.....	6
2.3.2	Potential applications of reversible heat engines	7
2.3.3	Overall concept of two cell RHEs	8
2.4	Methods	14
2.4.1	Cyclic voltammetry	14
3	Experimental	18
3.1	Cyclic voltammetry and temperature coefficient measurements.....	18
3.1.1	Equipment	18
3.1.2	Measurements.....	19
3.2	Heat battery tests	22
3.2.1	Equipment	22
3.2.2	Assembly of the heat battery setup	22
3.2.3	Measurements.....	24
4	Results and discussion.....	30
4.1	Cyclic voltammetry (CV) and the determination of temperature coefficients	30
4.1.1	Pseudo-reference hydrogen electrode	33
4.1.2	Platinum wire pseudo reference electrode.....	35
4.2	Heat battery results	37
4.2.1	Open circuit voltage – state of charge (<i>OCV-SOC</i>)	37
4.2.2	Polarisation measurements	42
5	Conclusion.....	48
6	References	49
7	Appendix	51
7.1	A1- Derivation of Q for the tested flow battery system	51

1 Introduction

The present energy production of the world will probably be doubled by 2050 in order to meet the energy demands for the increasing global population. Our society is more than ever before aware of sustainability issues. Due to limited fossil fuel resources and global climate change, any increase in energy production must be achieved without dramatic CO₂ emissions. Renewable energy sources are increasingly in use, due to the low cost of photovoltaic panels and wind mills. However, renewable energy sources, such as energy from windmills and photovoltaics are inherently intermittent [1].

Another approach to respond to ever increasing energy demand is to utilize the tremendous low-grade heat sources. Low-grade heat sources (<100 °C) are ubiquitous, generated in energy conversion and utilization processes. Additionally, one can create low-grade heat sources using Sun's energy. Among the methods for converting thermal energy to electricity, thermoelectric (TE) materials and devices have been studied extensively for several decades [2]. And although thermoelectric devices are attractive, there are limits in the physical nature of thermoelectric devices which results in relatively low efficiencies. In essence, thermoelectric devices are based on charge carriers: electrons in N-type materials and holes in P-type materials have the ability to move freely through metals and semiconductors. When temperature gradient is applied to thermoelectric devices charge carriers diffuse from hot to cold while carrying heat as well. The build-up of charge carriers is known as Seebeck effect, i.e. induced thermoelectric voltage in response to a temperature difference across that material. Also, this coupling of heat and electricity results in both heat and charge carrier flux in the device. However, provided heat is not efficiently converted into potential difference due to charge carriers not being able to 'carry' most of the heat and due to dissipation of heat along their path to the cold side. Further, some of the heat is also directly dissipated and lost in the lattice. It turns out that overall, in best thermoelectric materials, the conversion efficiencies do not exceed 10%. In other words, issues arise that the Seebeck coefficient, and thermal and electric conductivity properties are all effected by flow of electrons which conduct both heat and charge. Simply increasing the electrical conductivity simultaneously decreases the Seebeck coefficient and increases the thermal conductivity, limiting the potential improvement in efficiency [3].

An alternative approach is to explore thermodynamic cycles. It has been recently discussed that thermogalvanic cells could play a larger role in harvesting of low-grade thermal energy, such as waste heat cogeneration and low-temperature geothermal sources but also in solar thermal energy conversion systems. Most of the time, the Seebeck coefficient (α), Eq. 1., of thermogalvanic cells reaches three or four times that of solid thermoelectrics [4].

A thermogalvanic cell was defined by Agar [5] as “a galvanic cell in which the temperature is not uniform. In practice, such cell will consist of two metallic electrodes, not necessarily reversible or chemically identical, immersed in electrolyte, which may or may not be homogenous in composition, and in which selectively permeable membranes might be interposed”

For a half-cell reaction, $A + ne^- > B$, the temperature coefficient is defined as:

$$\alpha = \frac{\partial V}{\partial T} = \frac{\Delta S_{B,A}}{nF} \left[\frac{\text{V}}{\text{K}} \right] \quad (1)$$

where V is the electrode potential, T is temperature, n is the number of electrons transferred in the reaction, F is Faraday's constant and $\Delta S_{B,A}$ is the partial molar entropy change for the half cell reaction in isothermal condition. This effect indicates that the voltage of a battery depends on temperature; thus a thermodynamic cycle can be constructed by discharging the battery at T_1 and charging back at T_2 . If the charging voltage at T_2 is lower than the discharging voltage at T_1 , net energy is produced by the voltage difference, originating from heat absorbed at the T_2 temperature, similar to a thermomechanical engine with the Carnot efficiency as the upper limit. If these electrodes are connected to a load, electrical current and thus power can be delivered, thus converting thermal energy into electrical energy [6]. Thermogalvanic cells based on ferricyanide–ferrocyanide systems have been known to deliver the highest current and power output compared to other aqueous solution-based systems, due to their relatively high temperature coefficient, α , and the large current density associated with the redox couple [4]. And some studies, such as *Hu et al.* [6], have even demonstrated some potential real-world applications of thermogalvanic cells; for example, a thin and flexible cell that is designed to be wrapped around a pipe with cold (or hot) flowing liquid.

However, all of the above-mentioned configurations have been in one-cell-configurations with only one redox pair. Here the transport of heat and charge is fully coupled and suffers from very low conversion efficiency. In this work, we investigated the feasibility of a new two-cell electrochemical reversible heat engine (RHE) that can convert heat to electricity. Because the transport of heat and charge is fully decoupled, the conversion efficiency could be in theory optimised to the Carnot limit.

2 Theory

2.1 Flow batteries in general

Among the electrochemical energy storage technologies, flow batteries are unique, with liquid electrolytes that are stored separately from the electrochemical cells, which allows for the separation of energy and power, see Figure 1. Because of this unique configuration of a separate reactant storage and electrochemical reactor, a flow battery system (FBS) offers some key advantages relative to conventional batteries.

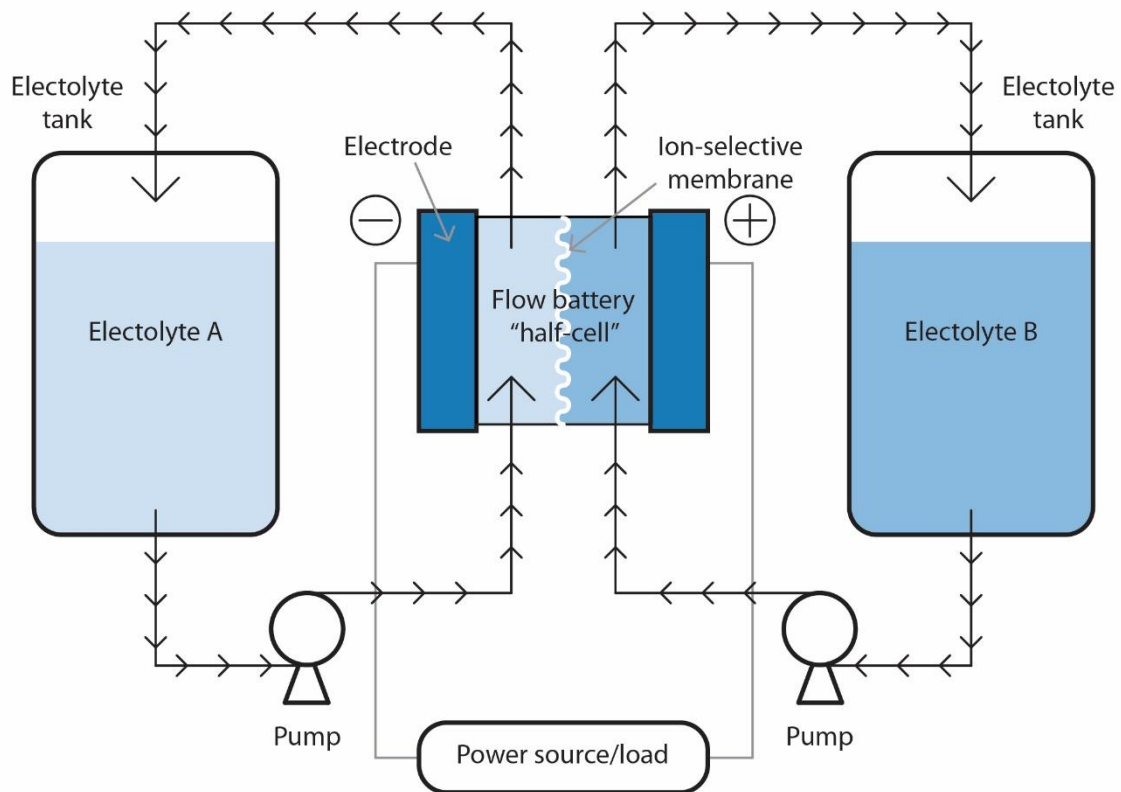


Figure 1. Basic flow battery layout.

FBS can be differentiated based on their active materials, i.e. their electrolytes. Flow battery electrolyte is typically composed of three species: a solvent, supporting electrolyte, and the active species, or redox couple. Redox reactions are reduction and oxidation reactions in which the oxidation states of molecules change. These redox reactions invariably involve the transfer of electrons, which are forced through the external circuit of a flow battery. To balance the electrons, and complete the circuit, ions are transported through the separator. These charge carrier ions are typically protons in the case of acidic electrolytes and either OH^- ions or potassium ions in the case of basic electrolytes [7].

Together with the most obvious advantage in FBS, like inherent design flexibility and safety because of its modularity, there are also some less obvious advantages of flow batteries. Since the active materials in flow batteries are stored in tanks, flow batteries can have extremely large

energy capacities without using thick electrodes. In other words, a flow battery can theoretically offer both high power density and large energy capacity in a single device, whereas the design of conventional batteries always entails a tradeoff between high power (which requires thin electrodes) or high energy (which requires thick electrodes).

Additionally, unlike conventional batteries, flow batteries are capable of reaching high depths of discharge without their cycle life being affected. During charging/discharging a conventional battery degrades over time because the active material is being expanded and contracted which limits their cycle life. However, since the changes in FBS are occurring in the active materials that are dissolved in liquid solutions their cycle life does not depend on the depth of discharge.

The electrochemical heart of FBs, like in the fuel cells, is the MEA (membrane electrode assembly), a sandwich consisting of two electrodes with an interposed polymeric membrane see Figure 2. In order to allow electrolyte flow toward the electroactive sites, the electrodes have a porous structure that can be obtained with carbon base materials such as carbon felt. These allow for porosity in the order of 0.8, thereby achieving a compromise between good electrode permeability and high electrode active area. However, since flow batteries reactions are completely reversible, unlike fuel cells, flow batteries use the same cell to operate as a converter of electricity into chemical energy and vice versa [8].

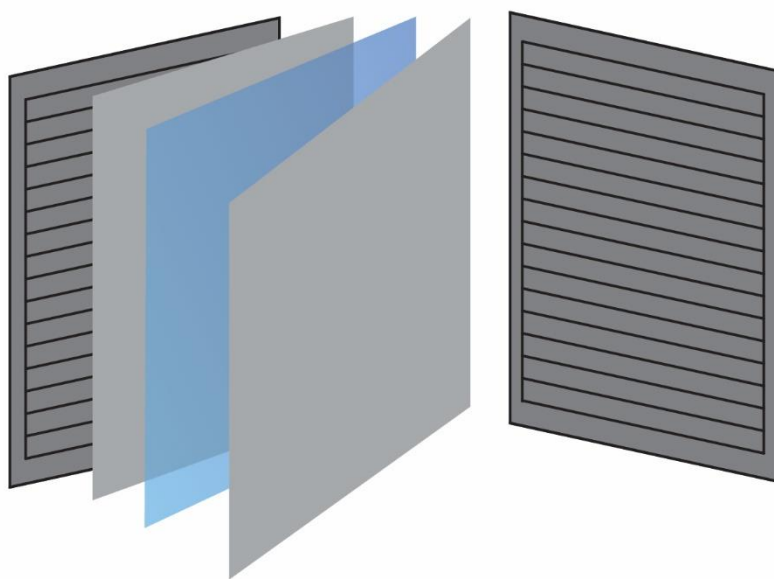


Figure 2. Diagram of a FB cell with MEA(membrane-electrode assembly)elements and bipolar plates with parallel-channel layout for flow-by distribution.

The open circuit voltage (*OCV*) of the cell is defined by the difference in the electrochemical potential of two redox couples. Therefore, these redox couples have a large influence on the performance of a FB, since not only does this determine the battery's key thermodynamic property (i.e., the *OCV*), but also the electrochemical reaction kinetics and the number of electrons per redox event, the chemical stability of the electrolytes, as well as the harshness of the chemical environment that the other battery components will be exposed to.

2.2 Cell potential of a flow battery

Charge and discharge curves of flow batteries, display Nernstian behavior, see Figure 3., where large changes in potential can be observed at the beginning of charging and discharging due to large relative concentration changes.

For an arbitrary electrochemical reaction



the behaviour is described with the Nernst equation

$$E_{cell} = E_{cell}^{\circ} - \frac{RT}{zF} * \ln \left(\frac{[C]^c [D]^d}{[A]^a [B]^b} \right) [V] \quad (3)$$

where E_{cell}° is the standard potential of the reaction, R the gas constant, T the absolute temperature in kelvin, z the number of electrons and F the faraday constant.

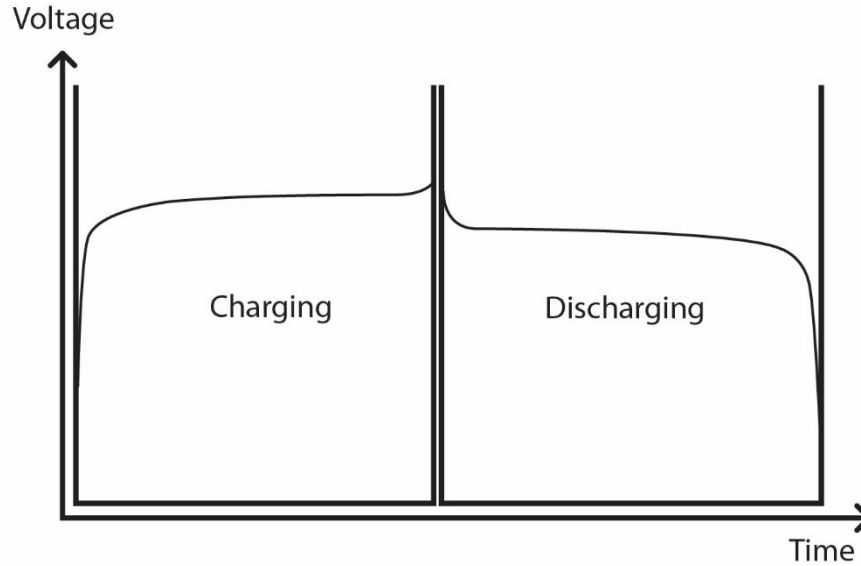


Figure 3. Nernstian behaviour of a battery when being charged and discharged

From the Figure 3. it can also be observed that the potential of the charging curve is higher than the potential of the discharge curve even though it is the same battery. This behaviour is assigned to the batteries internal and charge transfer resistance, where the potential of the battery during charging and discharging is described with Eq. 4 and 5.

$$U_{chg} = E_{cell} + I * R [V] \quad (4)$$

$$U_{dis} = E_{cell} - I * R [V] \quad (5)$$

In order to fully take advantage of the above mentioned thermogalvanic effects of redox pairs, in this work the feasibility of a double electrochemical flow cell for conversion of heat to electricity is investigated. This is essentially electrochemical heat engine with two flow cells that operate at different temperatures.

2.3 Heat engines

Heat engines are devices that convert heat into another form of energy, e.g. heat into electricity, or they can function in a reverse operation as heat pumps when energy, e.g. electricity, is put into the system, see Figure 4.

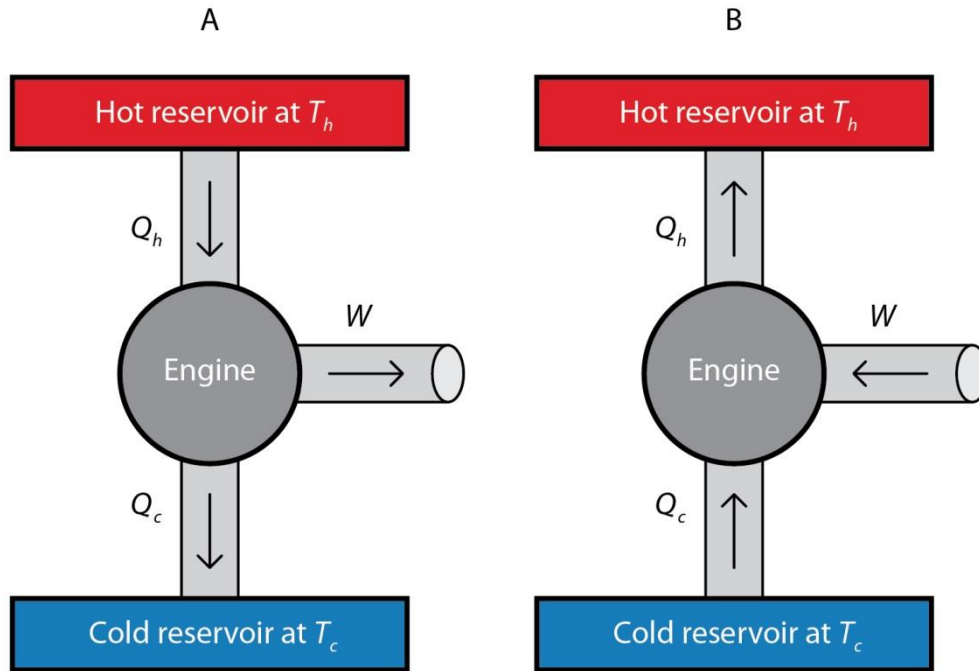


Figure 4. Thermodynamic representation of: A) a power generator that converts heat into electricity, and B) heat pump where heat is pumped from a cold to a hot reservoir.

2.3.1 General thermodynamics on heat engines

Any device which converts one form of energy into another can be described by its efficiency: the amount of energy input that is actually converted to useful output.

In all heat engines work/electricity is extracted from the flow of heat from a hot object to a cooler object, i.e. heat (Q_H) from a hot reservoir with temperature T_h enters the heat engine (system) where, because of the inevitable losses, a fraction is converted to electricity/work (P_{out}) and the rest of the heat (Q_C) leaves the heat engine to a cold reservoir with temperature T_C . From energy conservation it is clear that:

$$Q_H = W_{out} + Q_C \quad [J] \quad (6)$$

The conversion efficiency of the engine (η) for power generation, defined as the fraction of the ingoing heat energy that is converted to available work, is

$$\eta = \frac{W_{out}}{Q_H} = \eta_{RHE} \eta_C \quad (7)$$

Here η_{RHE} is the system efficiency of the heat-engine ($0 \leq \eta_{RHE} \leq 1$) and

$$\eta_C = (T_H - T_C)/T_H \quad (8)$$

is the Carnot efficiency. The Carnot efficiency is the maximum theoretical efficiency for a heat engine allowed by physical laws. Since the second law of thermodynamics states that all of the supplied heat in a heat engine can not be used to do work, the Carnot efficiency sets the limiting value on the fraction of the heat which can be so used.

In a heat-pumping mode, see Figure 4, an external work/electricity is applied to extract heat (Q_C) from a cold reservoir (T_C) through a heat engine to a hot reservoir (T_H) with a rate (Q_H). In this case energy conservation gives

$$Q_H = W_{In} + Q_C \quad [J] \quad (9)$$

A heat pump is subject to the same limitations from the second law of thermodynamics as any other heat engine. Here the efficiency is characterized by a coefficient of performance (COP), which is ratio of units of energy delivered to the hot reservoir (Q_H) per unit work (electrical) input (W_{In}) and given by

$$COP = \frac{Q_H}{W_{In}} = \eta_{RHE} COP_C \quad (10)$$

where

$$COP_C = T_H/(T_H - T_C) \quad (11)$$

is the maximum thermodynamic/theoretical COP value.

2.3.2 Potential applications of reversible heat engines¹

Figure 5 shows schematic examples of two fundamental integration possibilities of RHEs into a decentralised energy system. In the left example, during the day when energy is abundant, heat engine is used as a heat pump, thus all the surplus electricity that is produced via PV panel is used for driving heat engine that pumps heat from outside into a thermal reservoir. Heat from the thermal reservoir can be used for house utilities like heating and hot water in the building. Whenever no electricity is produced by the PV (e.g. during nights), the RHE operates as a generator that produces electricity from the heat reservoir. In this setup, the RHE functions as an electricity-heat-electricity conversion and storage device (i.e. combined heat-power-storage).

¹ Sections 2.3.2 and 2.3.3 were adapted from a note written by Bentien A., Aarhus University

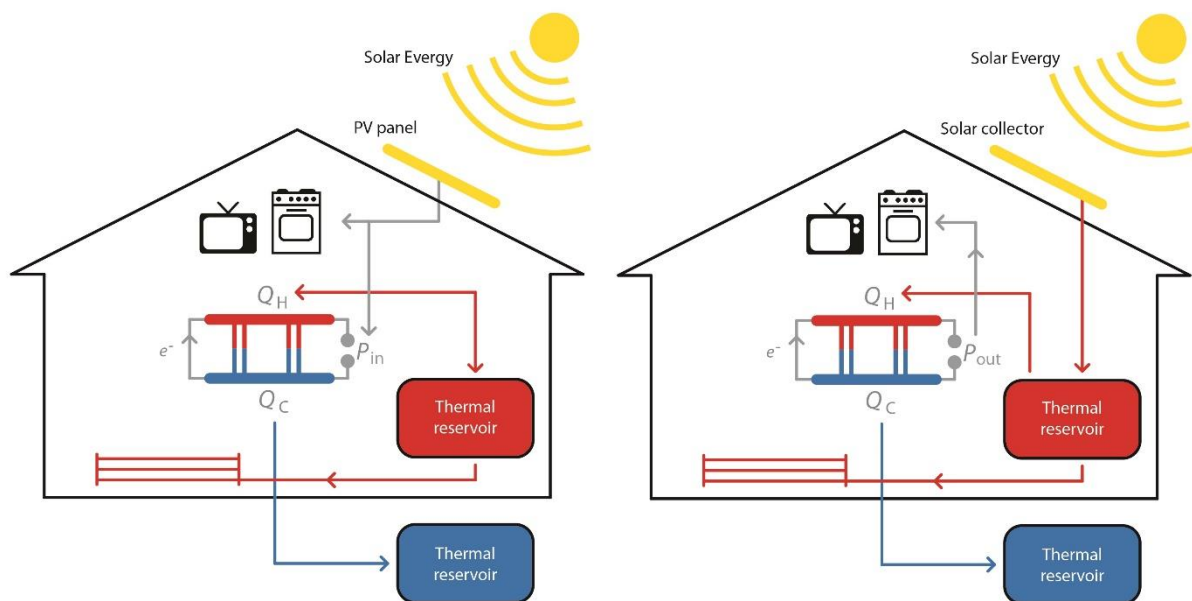


Figure 5. Schematic examples of integration of RHEs, where the RHE is symbolised as the blue/red figure with Q_H/Q_C . Left side shows the RHE in heat pump mode with PV panel, while the right side shows it in electricity generation mode with a solar heat collector

In the example on the right, see Figure 5, heat from a solar collector is stored in a thermal reservoir in the building and can be used for house utilities as well. In addition to this, heat from the thermal reservoir can also be converted into electricity when needed and the RHE functions as a heat-electricity conversion and storage device.

2.3.3 Overall concept of two cell RHEs ²

Figure 6. shows the basic concept of the electrochemical RHE during heat-to-electricity operation. It consists of two electrochemical flow cells (EFCs) that are connected to a heat reservoir at T_H and T_C respectively. In each EFC, redox solutions of e.g. $\text{Br}_2|\text{Br}^-$ and $\text{Fe}^{3+}|\text{Fe}^{2+}$ are circulated between the two sides of cells (indicated by the red/blue lines in the middle) that together carry a net amount of heat between the two EFCs and is quantified by $Q = K\Delta T$, where $K [\text{W K}^{-1}]$ is the thermal conductance and ΔT the temperature difference between the two EFCs.

² Sections 2.3.2 and 2.3.3 were adapted from a note written by Bentien A., Aarhus University

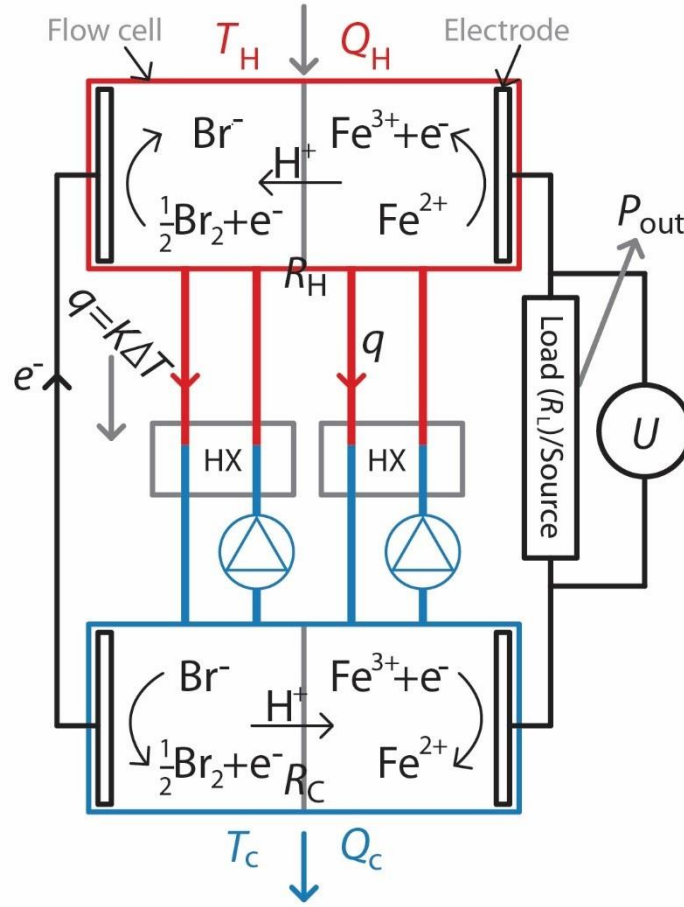


Figure 6. Schematic illustration of the new RHE based on two electrochemical flow cells at different temperatures. Dimensions and proportions are not to scale

The electrodes in both flow cells are connected electrically and electric work (W_{Out}) is extracted in an external load (R_L). During operation Br_2 and Fe^{2+} are reduced and oxidised in the hot cell, respectively, while the reverse reactions take place in the cold cell. Overall, this process corresponds to charging a redox flow battery at, e.g. low temperature, while discharging at high temperature. If the charging voltage at T_C is lower than the discharging voltage at T_H , net energy is produced by the voltage difference. Thus, electrical work can be extracted because the cell potential (E_{cell}) is higher at T_H than at T_C ($E_{cell}(T_H) > E_{cell}(T_C)$), meaning that it requires less energy to charge it at low temperature than what is discharged at high temperature. In other words, this means that cell needs to be charged at lower temperature, T_C , and discharged at higher temperature, T_H , when α is positive. In contrast, when α is negative, the cell needs to be discharged at lower temperature, T_C , and charged at higher temperature, T_H , where α is temperature coefficient, see Eq. 1.

Entire engine undergoes a thermal cycle containing four processes: heating up, charging, cooling down and discharging, see Figure 7. In process 1, the cell is e.g. in the discharged state and cooled from T_H to T_C (high to low temperature) at open circuit. The cell is then charged at low voltage at T_C in process 2, and the entropy of the cell increases through heat absorption during the electrochemical reaction. In process 3, the cell is disconnected and heated from T_C

to T_H , and thus the OCV increases. In the final process, the cell is discharged at a higher voltage at T_H , and the entropy of the cell decreases through the ejection of heat into environment and work can be extracted as the difference between charging and discharging energy.

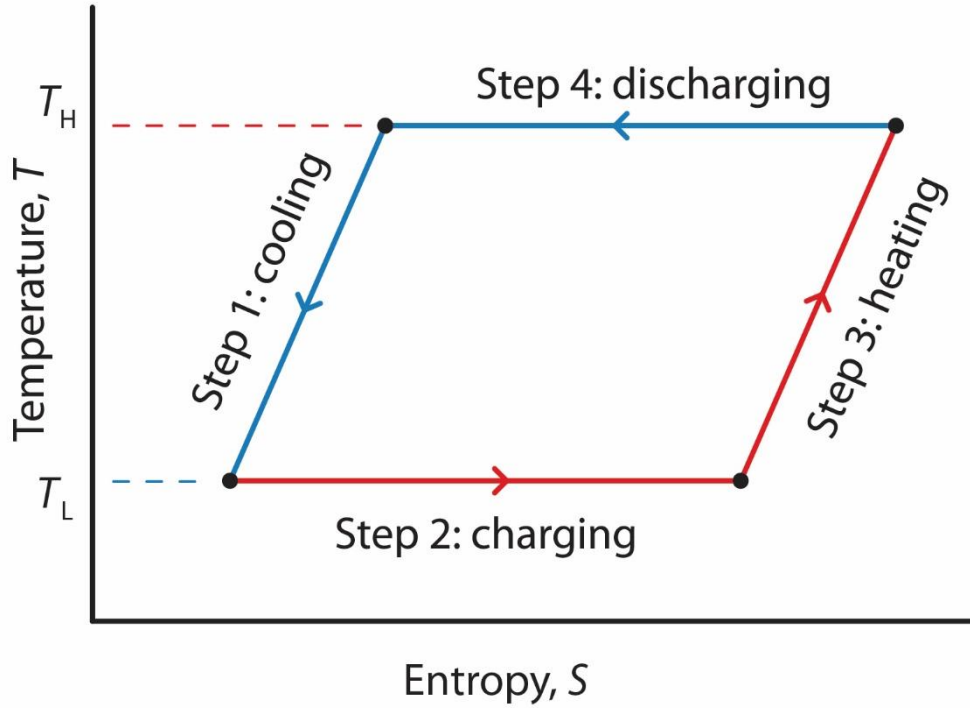


Figure 7. Temperature–entropy, (T–S), diagram of thermal cycling assuming a temperature range between T_L and T_H . The theoretical energy gained over one cycle is the area of the loop determined by the temperature difference and entropy change.

From a thermodynamic analysis the Gibbs Free energy change ($\Delta G(T)$) in each of the cells is given by

$$\Delta_r G(T, Q) = \Delta_r G^0(T) + RT \ln Q \quad \left[\frac{\text{J}}{\text{mol}} \right] \quad (12)$$

Where $\Delta_r G^0(T)$ is the standard reaction Gibbs free energy for the redox reactions in the cell and related to the standard reaction enthalpy ($\Delta_r H^0$) and entropy ($\Delta_r S^0$) through

$$\Delta_r G^0(T) = \Delta_r H^0 - T \Delta_r S^0 \quad \left[\frac{\text{J}}{\text{mol}} \right] \quad (13)$$

And Q is the reaction quotient for the redox reactions in e.g. $(AQ^{2-} + 2Fe(CN)_6^{3-} \rightarrow AQ_0 + 2Fe(CN)_6^{4-})$ and given by

$$Q = \frac{[AQ][Fe(CN)_6^{4-}]^2}{[AQ^{2-}][Fe(CN)_6^{3-}]^2} \quad (14)$$

The total amount of electricity/work that can be extracted from the RHE, without taking into consideration the losses, is given by the total Gibbs Free energy of both EFC ($\Delta_r G_{\text{RHE}}$) and found from

$$\begin{aligned}\Delta_r G_{\text{RHE}} &= \Delta_r G(T_H, Q_H) + \Delta_r G(T_C, Q_C) \\ &= \Delta_r G^0(T_H) + \Delta_r G^0(T_C) + RT_H \ln Q_H + RT_C \ln Q_C \left[\frac{\text{J}}{\text{mol}} \right]\end{aligned}\quad (15)$$

We can assume that the enthalpy change $\Delta_r H^0$ and the entropy change $\Delta_r S^0$ are the same at T_H and T_C , which is a good approximation when $\Delta T = (T_H - T_C)$ [K] is small, thus we get

$$\begin{aligned}\Delta_r G^0(T_H) + \Delta_r G^0(T_C) &= \Delta_r H_H^0 - T_H \Delta_r S_H^0 - [\Delta_r H_C^0 - T_C \Delta_r S_C^0] \\ &= -\Delta_r S^0(T_H - T_C) \left[\frac{\text{J}}{\text{mol}} \right]\end{aligned}\quad (16)$$

Here the minus sign before the bracket is because the reactions are reversed in the cold cell. Furthermore, it can be assumed that the concentration of the reactants and products are the same in both cells (the Soret effect can however make a small shift) whereby $Q = Q_H = Q_C^{-1}$ and it is found that

$$RT_H \ln Q_H + RT_C \ln Q_C = (T_H - T_C) R \ln Q \quad (17)$$

When eq. (16) and (17) are inserted into eq. (15), $\Delta_r G_{\text{RHE}}$ can be expressed as

$$\begin{aligned}\Delta_r G_{\text{RHE}} &= -\Delta_r S^0(T_H - T_C) + (T_H - T_C) R \ln Q \\ &= -(T_H - T_C)(\Delta_r S^0 - R \ln Q) \left[\frac{\text{J}}{\text{mol}} \right]\end{aligned}\quad (18)$$

Here it is seen that the amount of work ($\Delta_r G_{\text{RHE}} = W$) that can be extracted from the combined two-cell-system depends on the temperature difference, $\Delta T = T_H - T_C$, the reaction entropy and reaction quotient.

Physically, this effect (i.e. $\Delta_r G_{\text{RHE}}$) can be related to an open circuited thermogalvanic/thermoelectric voltage ($E_{\text{RHE}} = E_{\text{cell}}(T_H) - E_{\text{cell}}(T_C)$) that can be measured in the wires between the two cells and is related to $\Delta_r G_{\text{RHE}}$ through

$$E_{\text{RHE}} = -\frac{\Delta_r G_{\text{RHE}}}{nF} = \Delta T \frac{(\Delta_r S^0 - R \ln Q)}{nF} \text{ [V]} \quad (19)$$

Where n is the number of electrons in the redox reaction and F is the Faraday constant. By defining the Seebeck coefficient ($\alpha = \Delta U / \Delta T$, where ΔU is an electrical potential difference), Eq. (19) can be rewritten

$$\alpha = \frac{E_{\text{RHE}}}{\Delta T} = \frac{(\Delta_r S^0 - R \ln Q)}{nF} \text{ [V/K]} \quad (20)$$

To simplify equations (19) and (20), we can relate Q to the state-of-charge (SOC) of the solution (i.e. how much of e.g. Fe complex and AQ is in the charged state). It can be defined in many ways, however, here $SOC = \frac{[AQ^{2-}]}{[AQ]_0}$, where $[AQ]_0$ is the starting concentration of AQ and SOC gives the ratio of AQ on the 2⁻ form. With mass balances, see Appendix A1, it can be found that

$$Q = \frac{(1 - SOC)^3}{SOC^3} \quad (21)$$

In combination with Eq. (19) this is plotted in Figure 8, which shows the open circuit potential (E_{RHE}) of the RHE as function of the SOC with $\Delta T = 70$ K and $\Delta_r S^0 = 250 \text{ Jmol}^{-1}\text{K}^{-1}$. Here it is seen that E_{RHE} has a typical ‘Nernstian’ dependence on SOC .

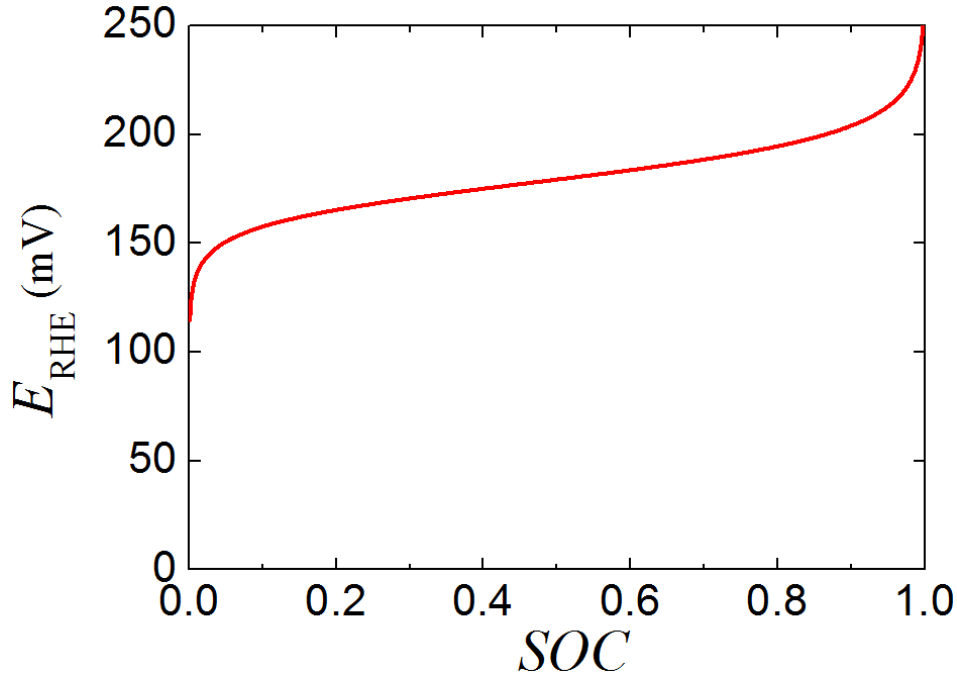


Figure 8. Calculation of E_{RHE} with $\Delta T = 70$ K and $\Delta_r S^0 = 250 \text{ Jmol}^{-1}\text{K}^{-1}$.

As mentioned above, the efficiency of the system (η) is calculated as the net work (W) divided by the thermal energy input. The energy input to complete the cycle includes two parts: the heat absorbed at T_H ($Q_H = T_H \Delta S$) and the external heat required to raise the temperature of the system (Q_{HX}). So in order to enhance the efficiency of electrochemical heat engine, heat recuperation system will be employed through tube in tube heat exchanger in order to harvest heat rejected through cooling process, thus remaining external heat that is required can be expressed as

$$Q_{HX} = (1 - \eta_{HX})C_P \Delta T \quad [J] \quad (22)$$

where C_P is the total heat capacity of the electrochemical cell and η_{HX} is the efficiency of the heat recuperation.

Consequently, η can be expressed as

$$\eta = \frac{W}{Q_H + Q_{HX}} = \frac{\Delta T(\Delta S - R \ln Q) - E_{\text{Loss}}}{T_H \Delta S + (1 - \eta_{HX})C_P \Delta T} \quad (23)$$

where E_{loss} is the energy loss due to the cell electrical resistance. Note that $\Delta T \Delta S = \alpha Q_C \Delta T$, where Q_C is the charge capacity of the battery cell [2].

The efficiency can be written as

$$\eta = \eta_c \frac{1 - \frac{R \ln Q}{\alpha Q_C} - \frac{I(R_H + R_C)}{|\alpha| \Delta T}}{1 + \frac{\eta_c(1 - \eta_{HX})}{|Y|}} \quad (24)$$

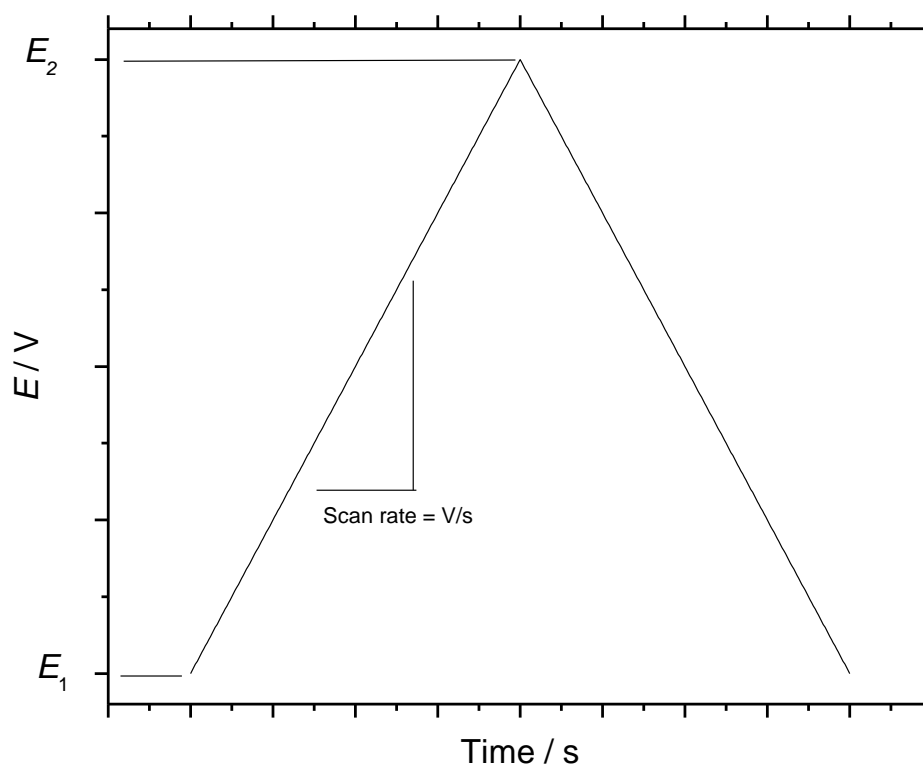
where I is the current used in discharging and charging. R_H and R_C are the internal resistance at T_H and T_C , respectively. $Y = \frac{\alpha q_c}{c_p}$, is a dimensionless parameter to describe the requirements of the system for high efficiency [2].

If only the contributions of the electrode materials are considered, and it is assumed that both electrodes have the same properties except opposite signs of the temperature coefficient, then $Y = \frac{\alpha q_c}{c_p}$ and it is defined as the figure of merit of an electrode material for RHE. Here, q_c is the specific charge capacity and c_p is the specific heat of an electrode. Consequently, it is clear that a higher temperature coefficient (α), a higher specific charge capacity (q_c) and a smaller specific heat (c_p) lead to higher efficiency for heat-to-electricity conversion. Further, it is worth noting that transport of heat and electricity in this system is fully decoupled, meaning that heat exchangers and flow cells can be optimised without affecting each other. So if the system has fast kinetics with low R and effective heat recuperation, overall efficiency of the system can additionally be improved.

2.4 Methods

2.4.1 Cyclic voltammetry

Cyclic voltammetry (CV) offers possibility of easily determining number of different thermodynamic and kinetic parameters for a number of different electrochemical reaction mechanism. The technique is ideal for preliminary tests and gathering data on the unknown systems, such as electrochemical mechanisms that occur in the system, identifying electroactive species, determining kinetic constants etc. The technique is most commonly utilized in three-electrode configuration in order to more accurately determine working electrodes potential. CV is an electrochemical technique which measures the current response as a function of applied voltage. The voltage is applied to the "working" electrode and is scanned linearly from an initial value, E_1 , to a predetermined limit, E_2 , (known as the switching potential) where the direction of the scan is reversed, see Figure 9.



Figur 9. Potential-time profiles used to perform cyclic voltammetry

Let us consider a simple redox process involving the transfer of one electron in a solution, as shown below



By sweeping the potential in a positive direction from E_1 to E_2 a process of oxidation will occur. As long as the applied potential is lower than the standard redox potential of the electroactive species only non-faradaic current can be detected, i.e. current due to the charging of solid/electrolyte interface. Further increase in the potential causes oxidation of electroactive species, which causes a concentration gradient of the electroactive species in the vicinity of the electrode. As the reduced form of electroactive specie gets more and more depleted, the concentration gradient continues to grow.

An application of Fick's First law of diffusion tells us that the current at any time is proportional to the concentration gradient for the reactant,

$$I = nFD \left(\frac{\partial c}{\partial x} \right)_{x=0} \quad (26)$$

The electrolysis of the reactant depletes its concentration near the surface. If we assume that the experiment is performed at a stationary electrode in an unstirred solution, then diffusion is the principal mode of transport of the reactant to the surface. This relatively slow mode of mass transport cannot maintain a steady state concentration profile in the region close to the electrode. Therefore, the depletion zone grows. In a sense, the average distance that the reactant molecules must travel to reach the surface increases. Consequently, the rate of mass transport decreases. Eventually the mass transport step becomes rate determining and at the moment when the concentration of the electroactive specie near the surface of the electrode reaches the value close to zero the current reaches maximum.

Further increase in potential to E_2 value causes no increase in current. Since all of the electroactive specie near the surface of the electrode has been depleted, the concentration gradient continues to decrease, thus causing the rate of mass transport to decrease and finally causing the current to decay. When the scan direction is reversed, the oxidized form is reduced back to the original starting material.

It is common practice to report the average of the forward and return peak potentials as the formal redox potential for the redox couple which includes some small corrections to the logarithm by taking into account activity coefficients and is the potential that is actually measured in an electrochemical cell. This is an approximation that is most accurate when the electron transfer process is reversible and the diffusion coefficients for the oxidized and reduced forms are the same. By reversible, electrochemists mean that the reaction is fast enough to maintain the concentrations of the oxidized and reduced forms in equilibrium with each other at the electrode surface [9].

The proper equilibrium ratio at a given potential is determined by Nernst Equation, see Eq. 3 where cell potential at standard conditions E_{cell}^0 is often replaced by the formal potential, $E_{cell}^{0'}$. Another characteristic of reversible systems is the dependence of the peak height on the square root of the scan rate, see Figure 10. At 25 °C the peak current is

$$I_p = (2,69 \times 10^5) n^{\frac{3}{2}} c_R A D^{\frac{1}{2}} \nu^{\frac{1}{2}} \quad [A] \quad (27)$$

where A [cm^2] is electrode surface, D [cm^2/s] is diffusion coefficient, ν [V/s] is scan rate, c [mol/cm^3] is concentration, and n is the number of electrons. As shown in Eq. 27., the peak height is proportional to the applied voltammetric scan rate and a plot of the peak height to the

square root of the scan rate should be linear [9]. Figure 10. depicts typical voltammetric profiles resulting from applying a range of scan rates. It is evident that each voltammetric signature is the same but that the current increases with increasing scan rate as predicted by Eq. 27. It is important to note that when the position of the current maximum occurs at the same potential with changing scan rate is characteristic of electrode reactions which exhibit rapid electron transfer kinetics, i.e. reversible electron transfer reactions.

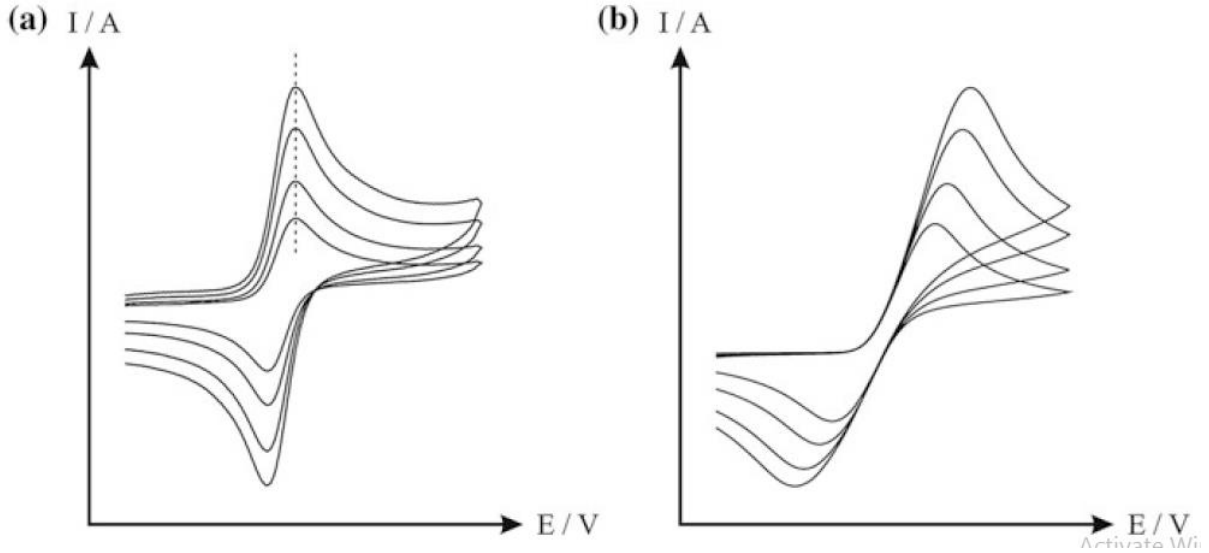


Figure 10. Reversible (a) and irreversible (b) cyclic voltammetric responses. Note the shift of the peak maxima with scan rate (The figure is taken from Ref. 10.)

Along with reversible reactions, there are irreversible and quasi reversible reactions which are all related to the rate of mass transport as well. In the case of quasi-reversible, the rate of electron transfer becomes comparable to the mass transport rate. In this regime, the peak potentials increase with the applied scan rate, see Figure 10b. Last, for the irreversible case the electron transfer rates are smaller than the rate of mass transport

Table 1. Diagnostic criteria for reversible, irreversible and quasi-reversible electrochemical processes

Reversible process	Irreversible process	Quasi-reversible process
$\Delta E_p = E_p^a - E_p^k = \frac{59}{n} (mV)$	No return peak	$\Delta E_p = E_p^a - E_p^k > \frac{59}{n} (mV)$
$\left \frac{I_p^a}{I_p^k} \right = 1$	$I_p^a \propto \nu^{1/2}$	$\left \frac{I_p^a}{I_p^k} \right = 1$ (for $\alpha_k = \alpha_a = 0,5$)
$I_p \propto \nu^{1/2}$	$\uparrow \nu \uparrow E_p^a (+30 \frac{mV}{f})$	$I_p \uparrow s \uparrow \nu^{1/2}$
$E_p \neq f(\nu)$	$ E_p - E_{p/2} = 48/f$	$E_p = f(\nu); (\uparrow \nu \uparrow E_p)$

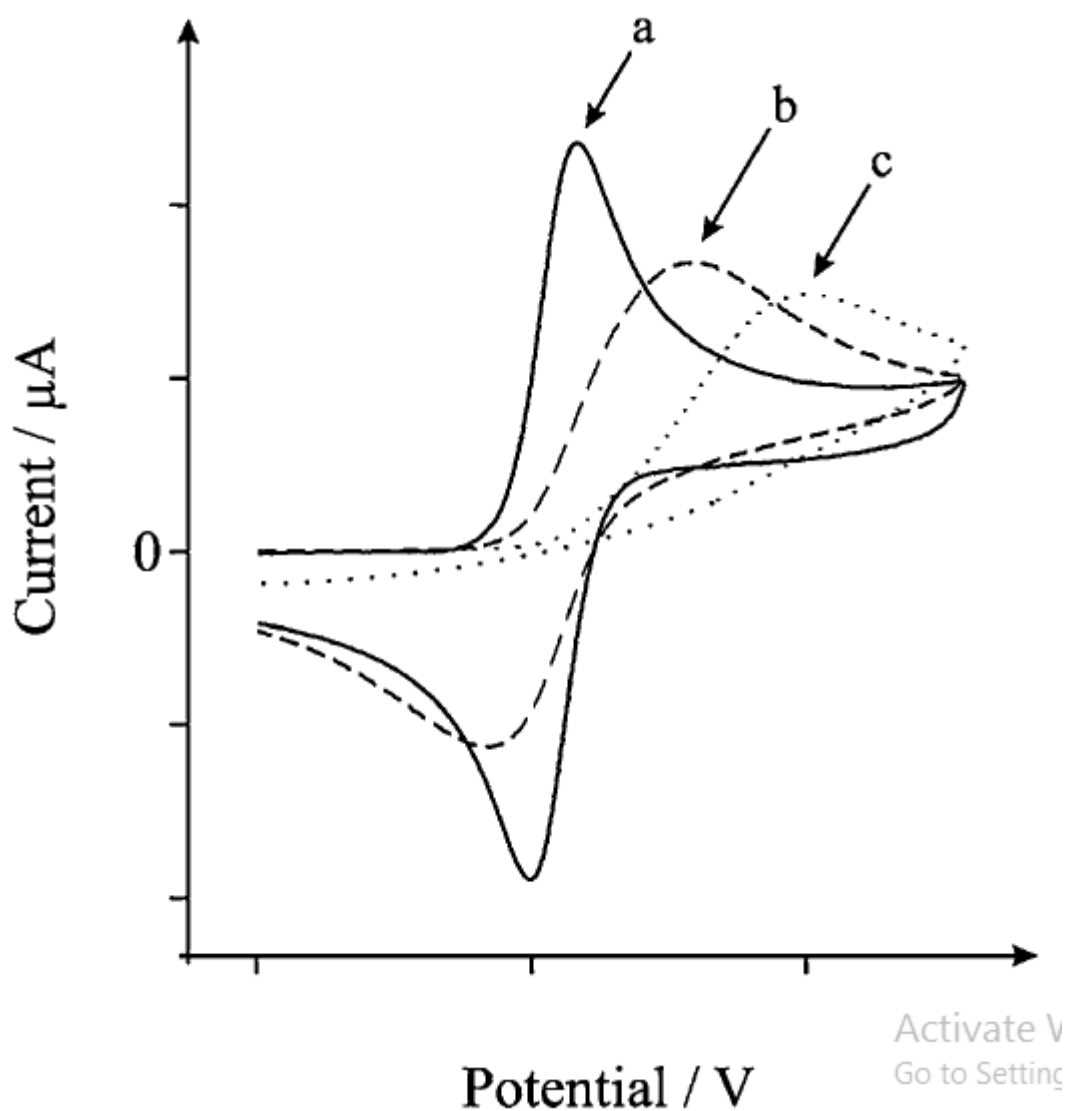


Figure 11. Cyclic voltammograms for reversible (a), quasi-reversible (b) and irreversible (c) electron transfer
(The figure is taken from Ref. 10.)

Also shown in Figure 11. is the cyclic voltammetric response for an irreversible electrochemical couple (in which ΔE_p is larger than that observed for the reversible and quasi-reversible case) where noticeable over-potentials are required to drive the reaction, as evident by the peak height occurring at a greater potential than that seen for reversible case [10].

In Table 1. are presented all of the parameters upon which can be decided if the electrochemical process is reversible, irreversible or quasi-reversible

3 Experimental

The experiments performed in this work present preliminary measurements on double electrochemical heat engine as a proof of principle and guidelines for future work.

The chemicals used in this work are given in Table 2.

Table 2. Compounds and chemicals that were used in the work

Compound	Abbreviation	Purity	Producer	CAS-number
2,6-dihydroxy-anthraquinone	DHAQ	95 %	AK Scientific	84-60-6
Anthraquinone-2,6-disulfonic acid disodium salt	AQDS	95 %	TCI Chemicals	853-67-8
Iron(III) chloride	FeCl ₃	99.99 %	Sigma-Aldrich	7705-08-0
Potassium hexacyanoferrate(II) trihydrate	K ₄ Fe(CN) ₆ x 3H ₂ O	98.5 %	Sigma-Aldrich	14459-95-1
Potassium hydroxide	KOH	90 %	Sigma-Aldrich	1310-58-3
Ammonium chloride	NH ₄ Cl	99.5 %	Sigma-Aldrich	12125-02-9
Bromine	Br ₂	99.99 %	Sigma-Aldrich	7726-95-6
Sulfuric acid	H ₂ SO ₄	ACS reagent, 95-98%	Sigma-Aldrich	7664-93-9
Sodium borohydride	NaBH ₄	95 %	TCI Chemicals	16940-66-2
Hydrogen peroxyde	H ₂ O ₂	30 % (w/w) in H ₂ O	Sigma-Aldrich	7722-84-1

3.1 Cyclic voltammetry and temperature coefficient measurements

3.1.1 Equipment

- Potentiostat, CH Instruments, CHI660e electrochemical workstation
- Glassy-carbon working electrode
- Platinum wire counter electrode
- Saturated Ag/AgCl reference electrode
- Pseudo-reference hydrogen electrode
- Double-wall pseudo-reference hydrogen electrode
- Platinum wire pseudo-reference electrode
- N₂ gas tank
- Pt100 electrode
- Keithley 2110 Series: 5½-Digit Dual-Display USB Multimeter

3.1.2 Measurements

In order to determine temperature coefficients, α , of individual redox pairs, cyclic voltammograms (CV) were recorded with a Chemical Instruments potentiostat (CHI660E) using standard three-electrode configuration consisting of a platinum wire counter electrode, 3 mm diameter glassy carbon working electrode (CHI) and a reference electrode in a glass beaker with custom built jacket that was connected to a heat bath to regulate the temperature, see Figure 12. Different self-made reference electrodes were employed throughout this work in order to obtain valid data on the thermogalvanic effects of the redox species. For each series of CVs, working electrode was freshly polished using polishing pads and alumina powders of 3, 1 and 0.05 μm in size, 3 min on each polishing pad.. Temperature in the cell was increased in steps by the use of water bath which had a built in internal pump, while being monitored with a Pt₁₀₀ temperature sensor that was connected to a multimeter. After each increase in temperature, a cyclic voltammogram was recorded.



Figure 12. Glass beaker with a jacket that was employed for CV measurements

Solutions were purged with N₂ (5.0 grade) prior to recording CVs. Scan rates of 0.05 V s⁻¹, 0.08 V s⁻¹, 0.1 V s⁻¹, 0.2 V s⁻¹ were used, however, only results for the 0.05 V s⁻¹ will be shown as no significant difference was noticed between different scan rates. Initial measurements were performed on a variety of active redox species. They were chosen based on their stated performance in the literature [11], if available, and on the feasibility of performing other measurements considering the inherent restrictions of the project itself (compatibility with a redox pair that is to be used on the other side and solubility of both species in the chosen supporting electrolyte). Measurements were conducted with 5 mM concentration solutions of Br₂, AQDS, Fe²⁺, K₄Fe(CN)₆ x 3H₂O, DHAQ in different supporting electrolytes.

Initial CV measurements were conducted with commercial Ag/AgCl (3M KCl) reference electrode with the potential of +0.215 V versus SHE and temperature coefficient of -0.13 mV/K [12]. With temperature coefficient in mind, adjustments to the reference electrode potential were done with temperature change.

3.1.2.1 Pseudo-reference hydrogen electrode

Hydrogen reference electrode offers sufficient accuracy for most electrochemical measurements, usually below 3 mV, for relatively concentrated acid or alkaline solutions. [13]

Custom made pseudo-reference electrode was designed by using Ag/AgCl reference electrode beaker that had Pt wire immersed in 1 M HCl aqueous solution. Beaker had specially designed tube on the side wall through which the H₂ was being continuously fed from a second beaker in which the NaBH₄ salt was used to create H₂, see Figure 13, and reaction below.



3.1.2.2 Platinum wire pseudo-reference electrode

The advantages of pseudo-reference electrodes being directly immersed into the electrolyte used in the cell is that the ohmic resistance effect is small, no liquid junction potential appears and usually there is no contamination of the test solution by solvent molecules or ions that a conventional reference electrode might transfer [14].

Platinum wire pseudo-reference electrode was prepared by directly immersing platinum wire into the cell with the electrolyte that is to be examined.

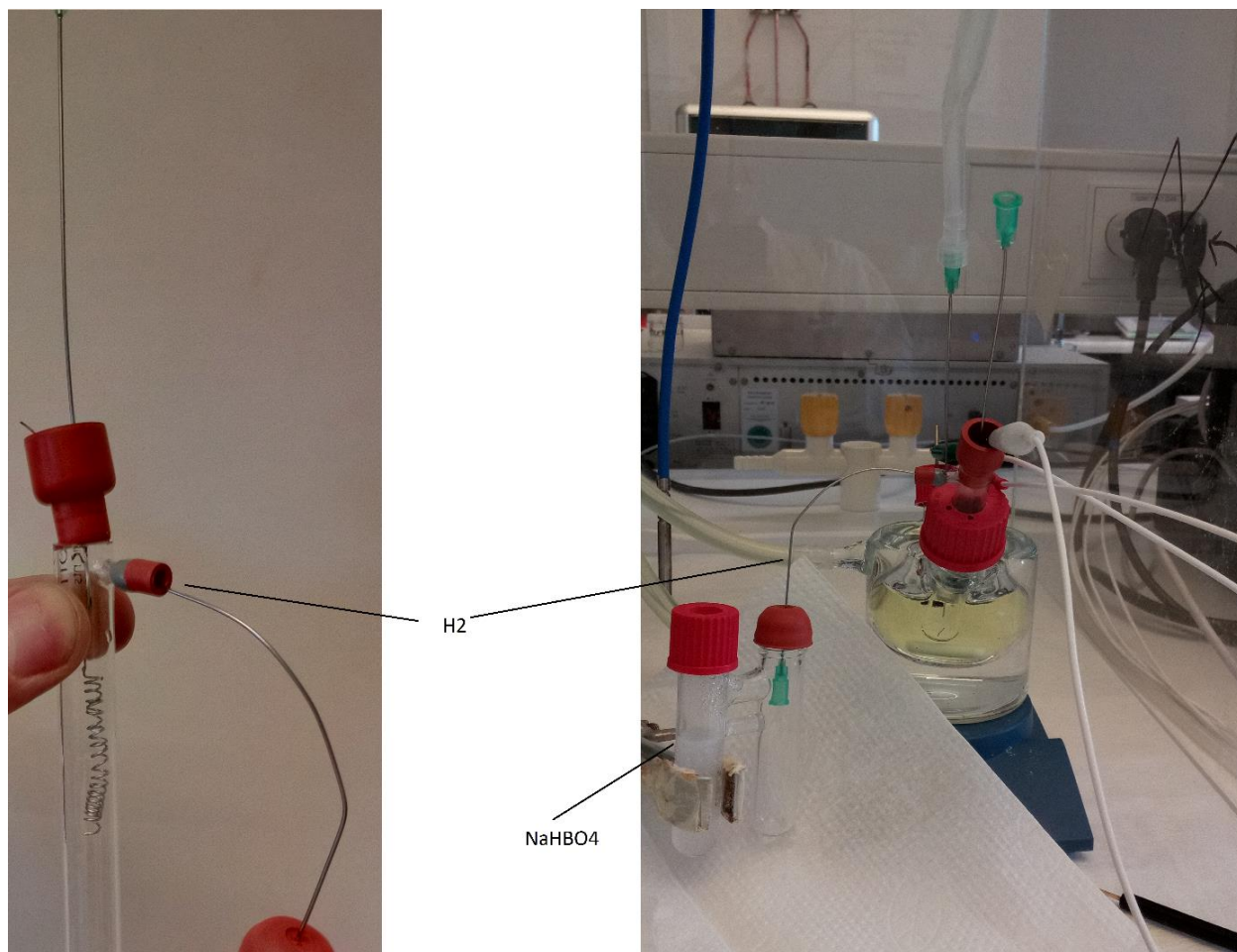


Figure 13. Custom built pseudo-reference hydrogen electrode

3.2 Heat battery tests

3.2.1 Equipment

- Neware BTS3000 (*battery testing station*)
Software:
BTS testing control 5.4.0013 (*testing software*)
BTSDA 7.4.1.3748 (*data software*)
- Thermolyne benchtop muffle furnace, ThermoFischer Scientific
- Carbon paper, 140 μm , Fuelcell Store
- Nafion 212 & 117 membrane, Fuelcell Store
- Lauda ECO E 4 S thermal bath
- N₂ gas tank
- Lindr CWP 100 Cooler
- Grundfos SMART digital DDA pump

3.2.2 Assembly of the heat battery setup

Figure 14. shows exploded view of the assembled electrochemical flow cell.

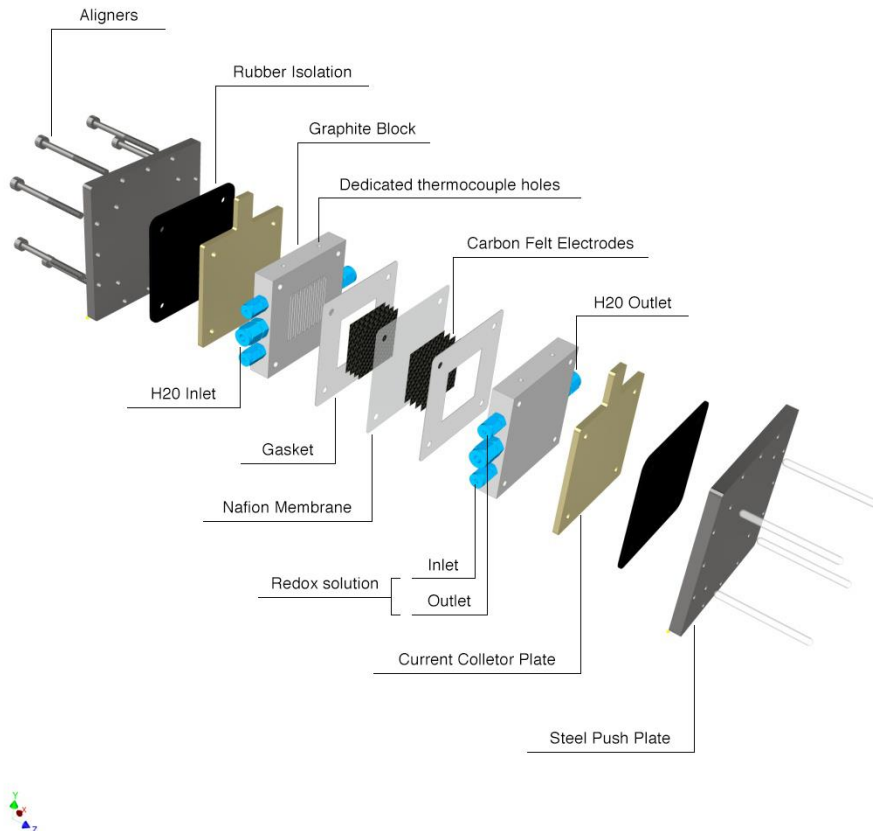


Figure 14. Exploded view of single cell with all of its components (Figure was adapted from references 20. and 21.)

Carbon paper was used as an electrode with high active surface area. 5 pieces of 140 μm thick and 25 cm^2 carbon felt electrodes were cut out from a sheet of carbon felt and pretreated by oxidizing them in a furnace at 410 $^{\circ}\text{C}$ for 3 h so they would become hydrophilic.

Nafion-212 membrane was used as an ion selective membrane. Membranes were pretreated in a following way: i) boiled for 30 minutes in a 3% H_2O_2 aqueous solution, ii) washed with miliQ water and iii) left soaking overnight in the 3M KCl aqueous solution to assure complete ion exchange of H^+ with K^+ ions in the membrane.

Rest of the space between graphite blocks was gasketed by 1 mm thick Teflon sheets.

The cells were interconnected with two heat baths, two pumps and a tube-in-tube heat exchanger as shown in the piping and instrumentation diagram (PID) diagram, Figure 15. One heat bath was used to adjust the temperature of the hot cell while the second heat bath was connected with the cooler and was thus used to maintain the temperature of the cold cell. Temperature in the cells was being monitored with K type thermocouples that were inserted in specifically designed holes on the side of the graphite blocks of the cells. Water flows from the heat baths were adjusted to enter the cells with a counter flow and so was the tube-in-tube heat exchanger. Electrolyte tanks were always purged with N_2 for 10 min prior to filling the system to ensure deaeration. After the system was filled with the solutions, tanks were cut off from the circulation through valves and the pump flow rates were adjusted to 3 L/h. Solutions have been kept circulating through the cells until stable temperatures have been achieved in both cells and then measurements were performed.

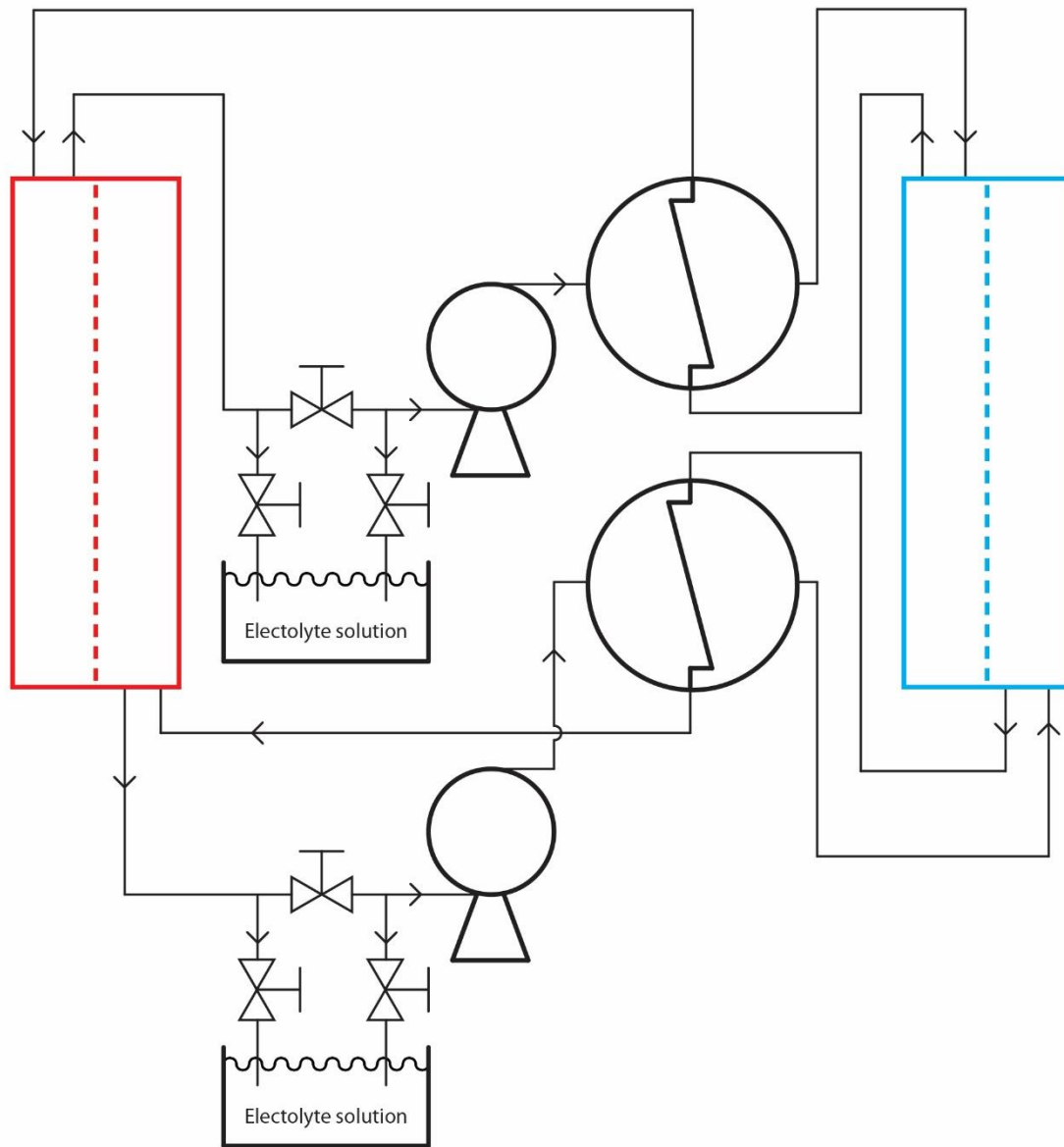


Figure 15. Piping and instrumentation (PID) diagram of heat battery setup. Note that heat baths are not represented, rather, hot and cold cells are indicated with red and blue color respectively

3.2.3 Measurements

Improved polarisation curves have been measured using BTS3000 battery tester (has 9 channels in total) in order to measure how much current can be drawn out of the system before the potential difference between the cells drops to zero. Usually, the linear part of polarisation curve can be used to estimate the internal resistance of the electrochemical cell, and in these experiments, voltage was measured as a function of the applied current. Thus, polarisation curves are helpful in explaining the chemistry and physics associated with flow cell operation, in a way that it gives rough estimation of the resistance of each cell [15]. Two battery tester channels were used to perform the improvised polarisation curve measurements. Cells were not

connected together, rather, each of them was connected to the battery tester individually where one channel was used for hot and one for cold cell and they were connected to them using four wire setup, as shown in the inset in Figure 16.. By doing so we were able to keep track of the potentials of the individual cells during measurements. Polarisation curves of the cells were performed at different *SOC* of the cells. The measurements were done so that hot cell was being charged in steps with currents of 5, 10, 25, 50, 75, 100, 125, 150 and 175 mA, while the cold cell was being simultaneously discharged with the same currents of the opposite sign and potential response was being recorded on both cells. The difference in potentials between the cells was calculated subsequently, as noted in the main Figure 16.

Further, *OCVs* of the individual cells were measured at different states of charge (*SOC*) in order to determine the potential difference that could be obtained between cold and hot cell at different *SOC*, as that is the driving force of the system, and all of these measurements were performed in a setup depicted in Figure 16.

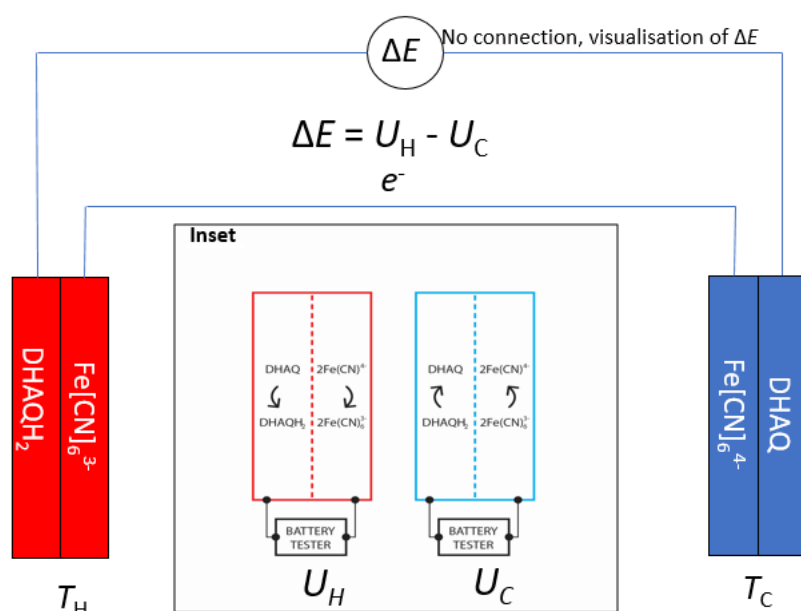


Figure 16. Individual cells connected to the battery tester. Red and blue cell represent hot and cold cell respectively. Charging was done through hot cell

The redox system of choice for heat battery measurements was a 2,6 - DHAQ for the negative side and $\text{K}_4\text{Fe(CN)}_6 \times 3\text{H}_2\text{O}$ complex for the positive side in two different concentrations with 1 M KOH as supporting electrolyte:

- 0.1 M 2,6 - DHAQ and 0.2 M $\text{K}_4\text{Fe(CN)}_6 \times 3\text{H}_2\text{O}$,
- 0.2 M 2,6 - DHAQ and 0.4 M $\text{K}_4\text{Fe(CN)}_6 \times 3\text{H}_2\text{O}$

3.2.3.1 Open circuit voltage – state of charge (OCV-SOC)

The system was charged through hot cell in steps, with currents in range of 250-500 mA in order to reach certain state of charge. State of charge can be calculated using Faraday's law, where

$$It = nzF \quad (29)$$

where I (A) is the with which the system is charged and t (s) is time of charging, while n (mol) is number of moles of electroactive species, z is number of electrons and F (C/mol) Faraday's constant. Because volume and concentration of redox species is known, it is possible to estimate state of charge, as

$$SOC = \frac{It}{nzF} \quad [\%] \quad (30)$$

System was also discharged in steps. In case of both charging/discharging only the potential difference was recorded in cold cell, as indicated in inset of Fig 16.. Between each step there was a resting period of 20 min. This was necessary to stabilize the potentials of the cells as it took time to circulate solutions from one cell to another. Measurements were done at different ΔT between the cells to obtain the data of the influence of ΔT on OCV-SOC curves of the heat battery.

Further, in order to exactly assess SOC values of the cells at various potentials, OCV-SOC calibration curve was obtained and model was fitted to it from measurements at room temperature for the 0.1 M DHAQ and 0.2 M $K_4Fe(CN)_6 \times 3H_2O$, where one cell was charged to 1.6 V and then discharged up to 0.5 V with currents of 500 mA for a couple of cycles, see Figure 17.

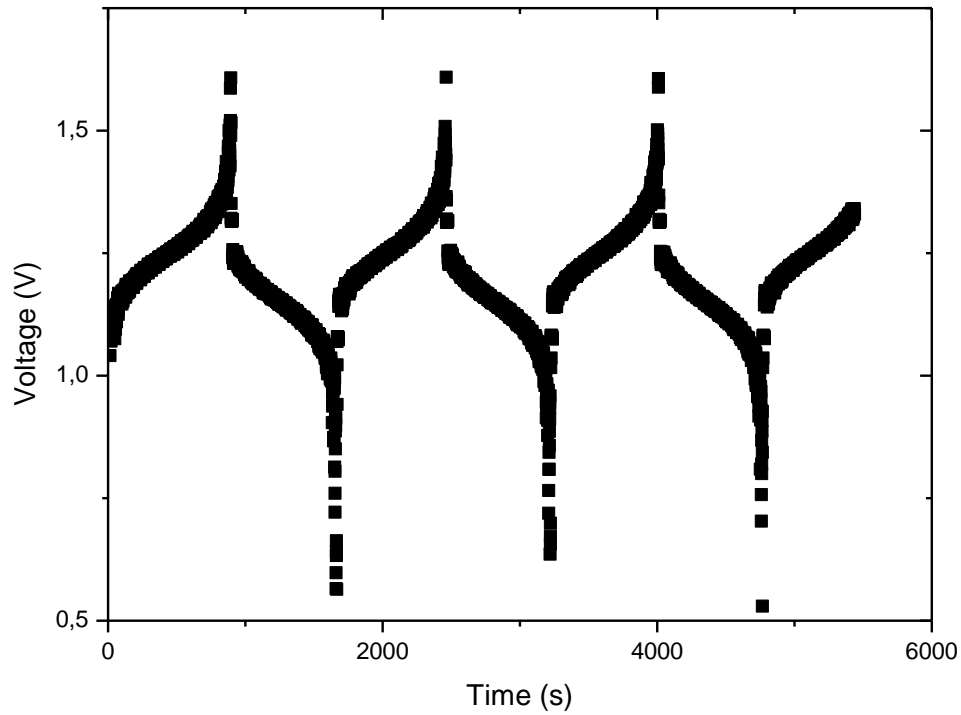


Figure 17. Charging and discharging of the cell at room temperature

To prove validity of the model, the correct *OCV-SOC* curve had to be obtained from the measurements. This was done in following steps.

Firstly, second cycle was taken as reference, and *SOC* values for it were obtained based on the amount of capacity with which the cell was charged in that particular cycle, while taking the value at 1.6 V as 100 % *SOC*.

Next, *OCV-SOC* curves were determined for the charging process and for the discharging process separately, while the values for discharging were inverted so they would match the ones from the charging process. Finally, the average of both charging and discharging process (inverted) was calculated and final *OCV-SOC* curve was obtained, see Figure 18.

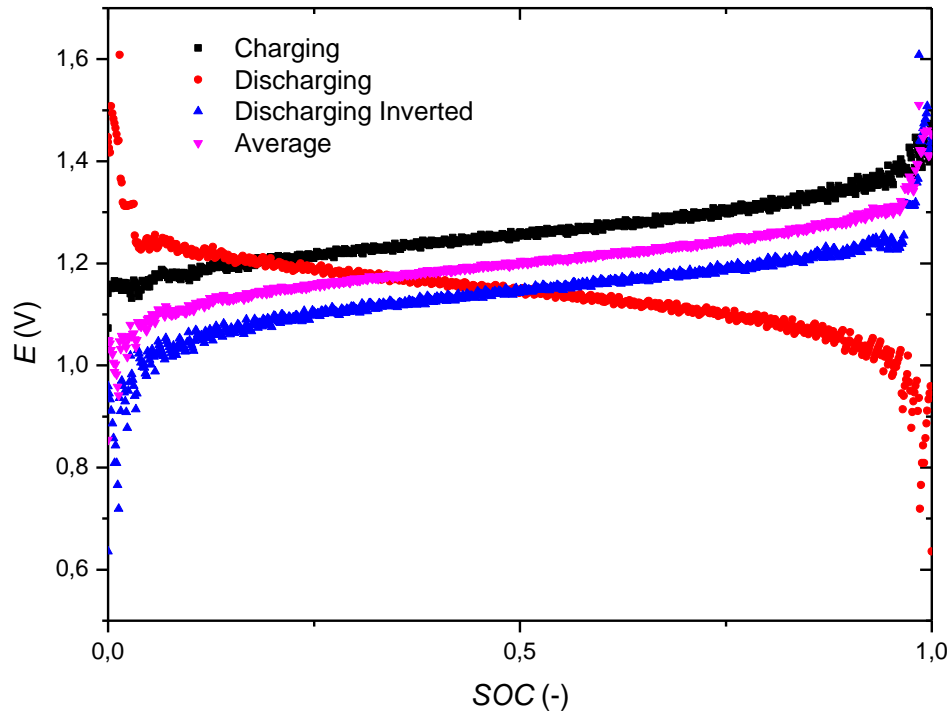


Figure 18. *OCV-SOC* curves for individual charging and discharging, and average of both. Model based on the Eq. 31. was fitted to the final curve.

$$E = E^0 - \frac{TR}{nF} \ln \left(\frac{1 - SOC}{SOC} \right)^3 \quad [\text{V}] \quad (31)$$

where $E^0 = 1.201279 \text{ V}$ is standard cell potential of the system, see Figure 19.

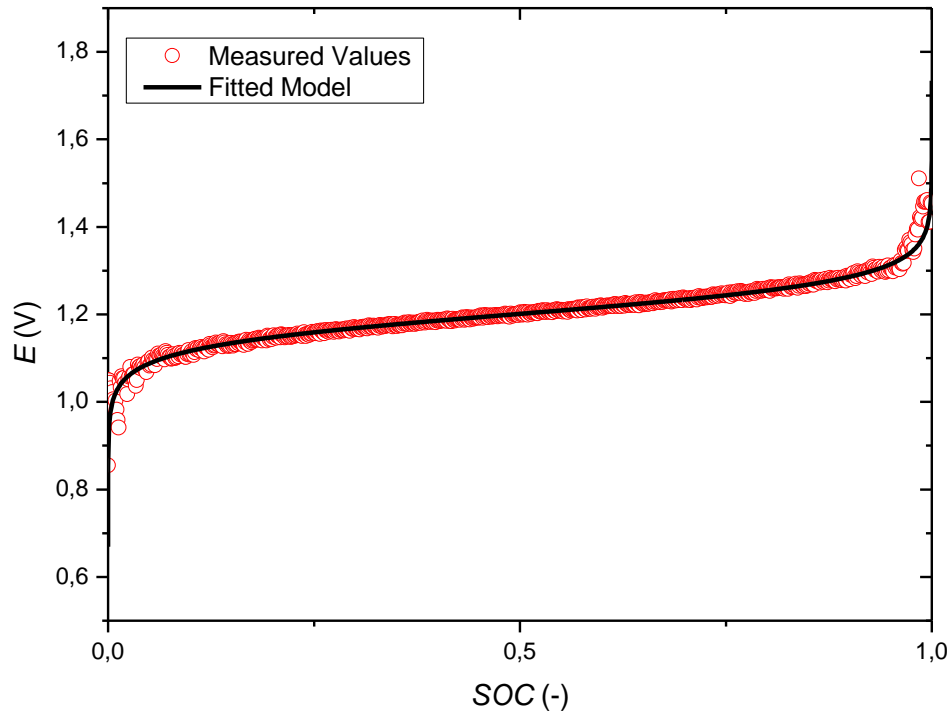


Figure 19. Fitted model from Eq. 31. to the *OCV-SOC* curve.

Model is showing good fitting for *SOC* values above 5 % and bellow 95 %. This model is used in further analysis of the data for the determination of the exact states of charge of the cells.

Measurements were conducted at two temperature differences for both redox system, i.e. $\Delta T = 30\text{ }^{\circ}\text{C}$ ($T_{\text{COLD}} = 25\text{ }^{\circ}\text{C}$, $T_{\text{HOT}} = 55\text{ }^{\circ}\text{C}$) and $\Delta T = 50\text{ }^{\circ}\text{C}$ ($T_{\text{COLD}} = 25\text{ }^{\circ}\text{C}$, $T_{\text{HOT}} = 75\text{ }^{\circ}\text{C}$), with an additional temperature difference for the measurements with lower concentrations, $\Delta T = 35\text{ }^{\circ}\text{C}$ ($T_{\text{COLD}} = 10\text{ }^{\circ}\text{C}$, $T_{\text{HOT}} = 45\text{ }^{\circ}\text{C}$).

4 Results and discussion

4.1 Cyclic voltammetry (CV) and the determination of temperature coefficients

In order to assess which redox pairs would be the most suitable for the heat battery engine it is necessary to determine temperature coefficients of individual redox pairs. Temperature coefficients were measured by cyclic voltammetry (CV) method, where temperature has been increased in steps and a cyclic voltammogram was recorded after each step.

From each CV a formal redox potential $E^{0'}$ was determined. The value of $E^{0'}$ is close to the standard redox potential, while taking into account activity coefficients of the reactants, Eq. 32. $E^{0'}$ was determined as the midpoint potential between the two peak currents, i.e. anodic and cathodic peak currents from the cyclic voltammograms.

$$E^{0'} = E^0 + \frac{RT}{zF} \ln \frac{\gamma_{ox}}{\gamma_{red}} \quad (32)$$

Figure 20. shows the cyclic voltammograms of three redox pairs of the potential interest for flow cell applications (AQDS/AQDSH₂, Br₂/Br⁻, Fe³⁺/Fe²⁺). All redox pairs are characterized by both anodic current peak and their cathodic counterparts. The highest current was registered for Br₂/Br⁻ redox couple since the measurements were carried out in the solution of 0.1 M HBr while the concentration of other two redox pairs were 5 mM only. As determined from anodic and cathodic peak separations, among the three investigated redox couples, AQDS/AQDSH₂ redox couple shows fastest charge transfer kinetics making it a system of choice for the high power applications. Br₂/Br⁻ and Fe³⁺/Fe²⁺ exhibit higher irreversibility. On the other hand, from the stored energy point of view, Br₂/Br⁻ redox pair would be most suitable redox pair for flow cell applications due to highest formal oxidation potential. From the investigated redox pairs, the largest difference of redox potentials was observed between AQDS/AQDSH₂ and Br₂/Br⁻ making them suitable pairs for the anolyte and catholyte in flow cells, respectively.

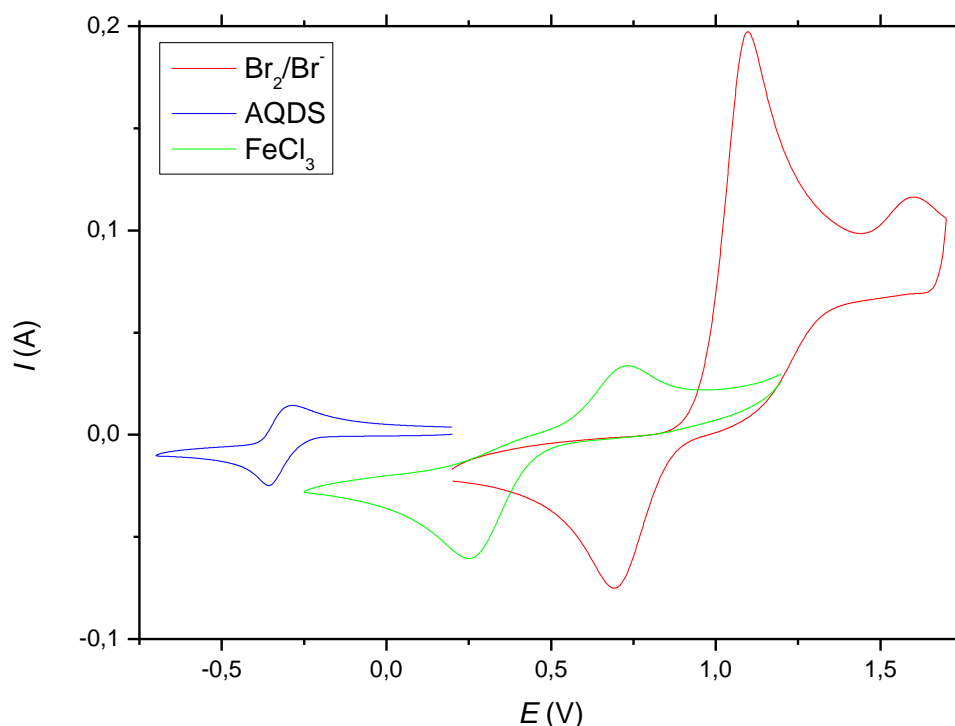


Figure 20. Cyclic voltammogram of 5 mM AQDS in 1 M HCl, 5 mM FeCl₃ in 1 M NH₄Cl, 50 mM Br₂ / 0,1 M HBr in 1 M H₂SO₄ at 25 °C

As mentioned in section 3.2.2., different reference electrodes have been used for CV measurements, some of them being commercial reference electrodes and some self made. Together with the choice of the reference electrodes, the choice of redox pairs was being decided along the measurements and thought process on this will be discussed throughout this section.

For the electrochemical reversible heat engine it is important to ensure that the selected redox pairs have large temperature coefficient, α , in order to secure as large energy content as possible. Our measurements were further focused on their determination by cyclic voltammetry. From the literature values of the temperature coefficient of the investigated redox pairs [11,16] ($\alpha_{\text{Br}_2|\text{Br}^-} \approx -1$ to -5 mV/K, $\alpha_{\text{Fe}^{3+}|\text{Fe}^{2+}} = 1.2$ mV/K), it would be reasonable to assume that if these two redox pairs were put into electrochemical heat engine, a value of $\alpha = \alpha_{\text{Fe}^{3+}|\text{Fe}^{2+}} - \alpha_{\text{Br}_2|\text{Br}^-} \approx 5$ mV/K could be reached. Therefore, these redox pairs have been chosen for initial CV measurements to examine their behaviour with the temperature change. It is also interesting to examine AQDS behaviour in regards to temperature change as recent work has proved its usability in flow batteries [17].

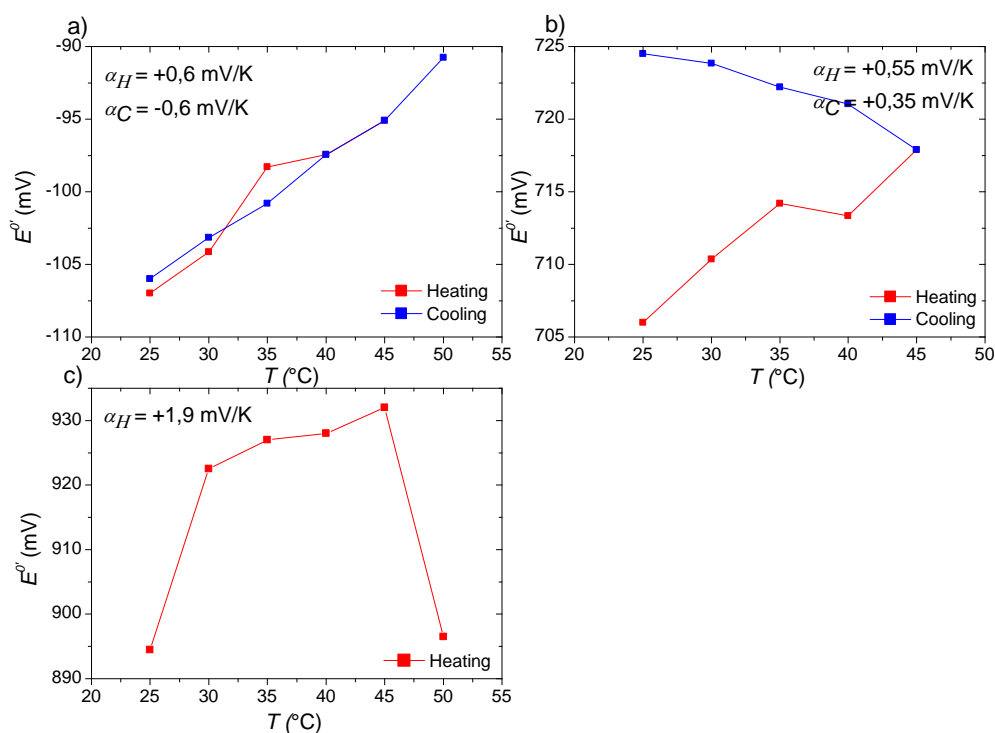


Figure 21. Thermogalvanic measurements for the solutions of: a) 5 mM AQDS in 1 M HCl b) 5 mM FeCl₃ in 1 M NH₄Cl, c) 50 mM Br₂ / 0.1 M HBr in 1 M H₂SO₄

Values of 0.6 mV/K were measured for the AQDS/AQDSH₂ redox pair, far less when compared to the literature values of 1-5 mV/K for the Fe²⁺/Fe³⁺ and Br₂. Further, Fe²⁺/Fe³⁺ potential values continued to change in the positive direction even after the temperature change has been shifted in the opposite direction, i.e. from heating switched to cooling. On the other hand, for Br₂/Br⁻ redox pair unknown reactions were observed at higher temperatures and at more positive potentials, as can be seen from recorded CV's, see Figure 22. At the 50 °C there was a huge potential drop and black precipitation was noticed in the cell. Cooling was not done after that.

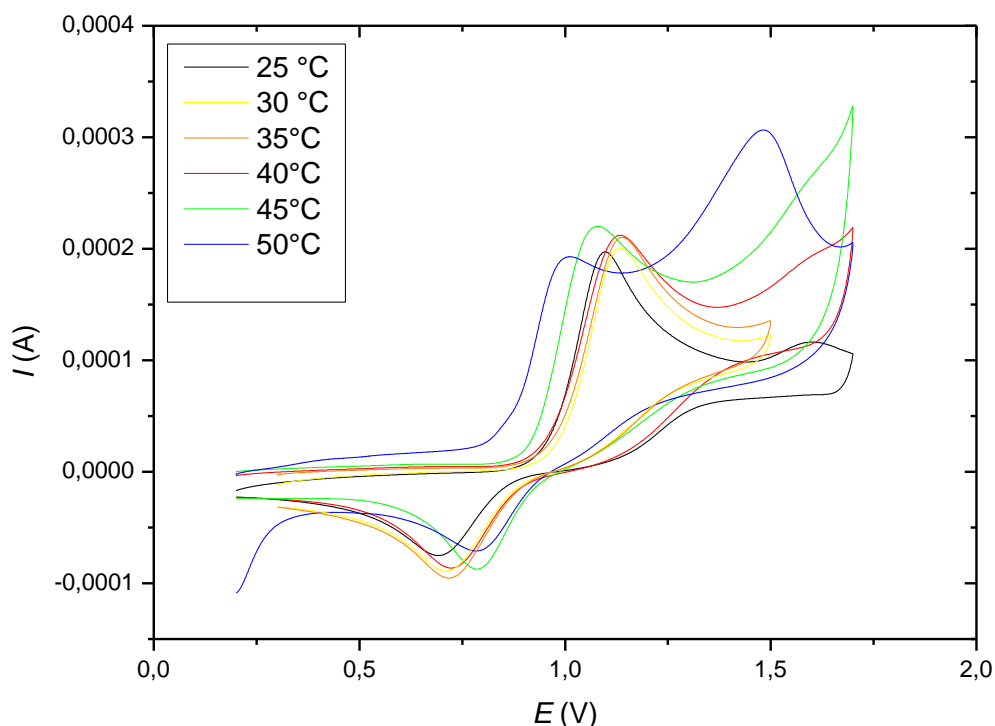


Figure 22. Recorded CV's for the 50 mM Br₂ / 0,1M HBr in 1M H₂SO₄

High temperatures pose additional challenges that need to be taken into consideration when doing CV measurements. Thus, further measurements were made with a custom-built pseudo reference hydrogen electrode in order to neglect these numerous difficulties.

4.1.1 Pseudo-reference hydrogen electrode

Because of toxicity concerns, and because it would require further technical precautions that would only add to the complexity of the measurements, Br₂/Br⁻ redox couple was not investigated anymore from this point of the project.

Instead, bromine could be replaced with the nontoxic ferrocyanide ion (known food additive) in an alkaline solution. The use of ferrocyanide offers notable advantages over bromine because it is nonvolatile and noncorrosive, allowing simpler and less expensive materials of construction [18]. Further, quinone-based redox species can also be adapted to alkaline solutions, where hydroxylated anthraquinones are highly soluble. In alkaline solution, OH⁻ groups are deprotonated to provide solubility and greater electron donation capability. Commercially available 2,6-dihydroxyanthraquinone (2,6 – DHAQ) has already been used in alkaline quinone flow batteries by *K. Lin at al.* [18] and they have reported the ability of hidroxy-substituted anthraquinone and ferrocyanide to function as stable flow battery electrolytes in alkaline solution

The obtained results were shown in Figure 23 as a dependence of formal redox potential, E^0 , determined by cyclic voltammetry on temperature.

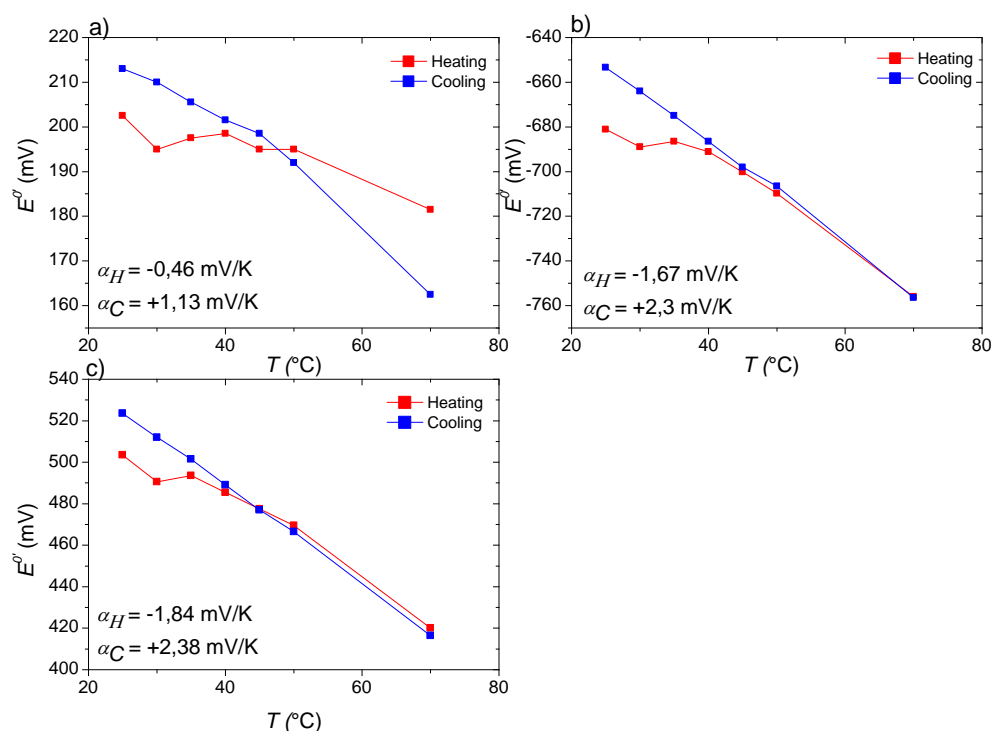


Figure 23. Thermogalvanic measurements for the solutions of: a) 5 mM AQDS in 1 M HCl b) 5 mM DHAQ in 1 M KOH, c) 5 mM $K_4Fe(CN)_6 \times 3H_2O$ in 1 M KOH

At first, results seem to be relatively good, especially with DHAQ and ferrocyanide, both showing α values well above 1 mV/K. However, AQDS values are very different from those measured with Ag/AgCl reference electrode, meaning that the sign of potential change has been reversed. With Ag/AgCl reference electrode AQDS showed positive change of +0.6 mV/K for heating, while, on the other hand, it is showing negative change of -0.46 mV/K for heating with pseudo-reference electrode. Further, if a closer look is taken at the shape of the curves from all three measurements, an odd similarity can be noticed, especially for the measurements with DHAQ and ferrocyanide, even in the terms of α values.

Since there are two different chemical compositions in the cell, one being 1 M KOH solution and other being 1 M HCl solution in the pseudo-reference electrode, it was assumed that only potential change due to cross-over of H^+ ions through walls of the pseudo-reference electrode has been measured.

In attempt to avoid this diffusion of ions through the walls of the reference electrode, following measurements were conducted while placing the reference electrode in the solution for only short periods of time. In other words, when there is a process of heating/cooling of the solution going on until stable temperatures were achieved, the reference electrode was being held outside of the cell. Once the stable temperatures were achieved, reference electrode was put in to the cell, and the measurements were performed. After that electrode was taken out and rinsed and new cycle begins.

Also, all further CV measurements were performed only on DHAQ or ferrocyanide complex because at this point of the project they were chosen as the redox pair for heat battery tests and because of the time limitations.

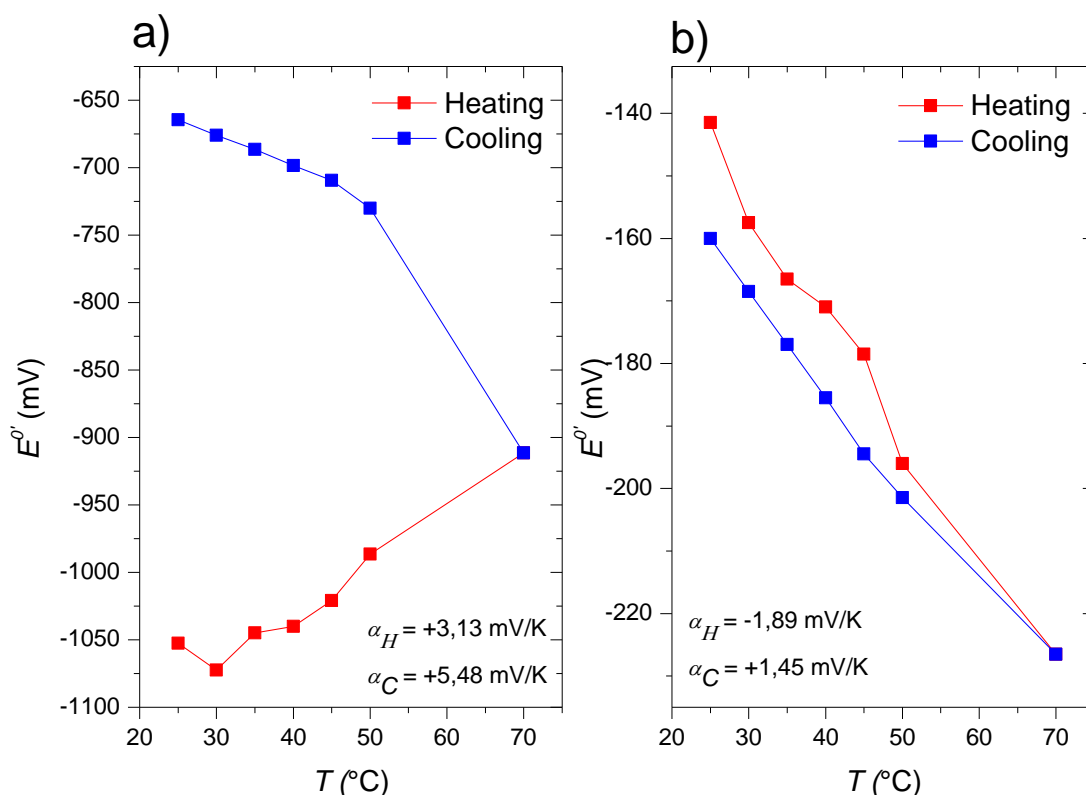


Figure 24. Thermogalvanic measurements for the solutions of: a) 5 mM DHAQ in 1 M KOH, b) 5 mM $\text{K}_4\text{Fe}(\text{CN})_6 \times 3\text{H}_2\text{O}$ in 1 M KOH

Though DHAQ showed relatively big α values for heating, the same problem appeared again as with the measurements for the $\text{Fe}^{2+}/\text{Fe}^{3+}$ redox pair with the Ag/AgCl reference electrode, where the potential values continued to change in the same direction even after temperature change has been shifted in the opposite direction, i.e. from heating switched to cooling. Interestingly, on the other hand, ferrocyanide complex is showing similar results as previous measurements with pseudo reference electrode, which are in good agreement with literature values, however there is no characteristic shape of the curve that was noticed for the previous measurements.

4.1.2 Platinum wire pseudo reference electrode

Kaseem et al. [19] showed that under certain conditions, such as high temperatures, where the usual reference electrodes cannot be used in electrochemical measurements, Pt wire is a satisfactory reference electrode.

The obtained results were shown in Figure 25 as a dependence of formal redox potential, E^0 , determined by cyclic voltammetry on temperature.

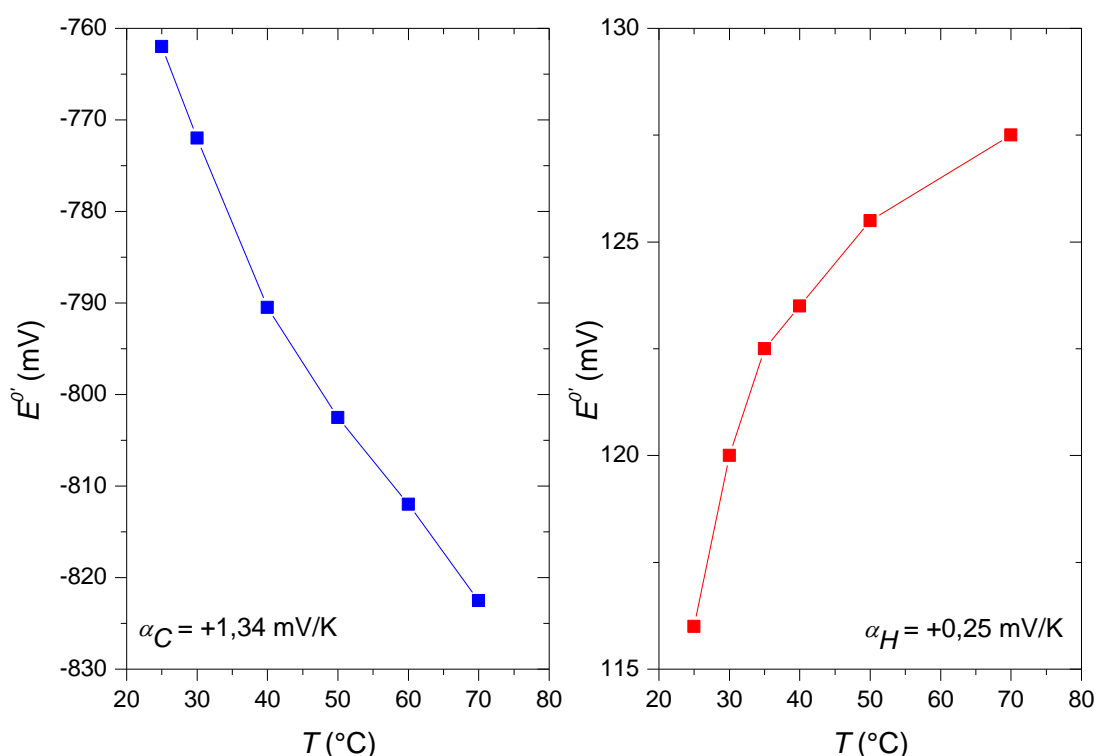


Figure 25 Thermogalvanic measurements for the solutions of: a) 5 mM DHAQ in 1 M KOH, b) 5 mM $\text{K}_4\text{Fe}(\text{CN})_6 \times 3\text{H}_2\text{O}$ in 1 M KOH

The results are not showing characteristic shape that was noticed for the measurements with the hydrogen pseudo-reference electrode. However, α values obtained with the Platinum wire reference electrode are far smaller than what has been measured up to this point. Further, it can be seen from the figure that the α value for the ferrocyanide has been shifted, in this case for heating, from negative to positive sign.

However, this shift in the value, if taken as true, is beneficial for the heat engine as opposite signs of α values should result in bigger heat to energy conversions.

Lastly, CV measurements and determination of temperature coefficients has proved to be challenging task with numerous obstacles. Stability of the electrolytes at higher temperatures need to be well understood, together with stabilities of compounds and solutions that are used in the reference electrodes themselves to avoid unwanted reactions and contamination of examined electrolytes. For that reason, inert elements such as Platinum have to be considered.

Though it is not possible to confirm which CV measurements are giving correct results, it is plausible that Platinum wire might be the best choice because of its inertness. Further, there is additional benefit to using Platinum wire as a reference electrode, i.e. liquid junction that usually exists between reference electrode and examined electrolyte is avoided. When conducting measurements at higher temperatures this proves to be crucial.

4.2 Heat battery results

Upon deciding on the appropriate redox system that was to be used for heat battery, i.e. 2,6 - DHAQ- $\text{K}_4\text{Fe}(\text{CN})_6 \times 3\text{H}_2\text{O}$, the heat-battery engine was assembled and the thermodynamic and kinetic measurements were conducted. All the measurements and analysis follow the methods described in section 3.2.3

4.2.1 Open circuit voltage – state of charge (*OCV-SOC*)

In order to assess basic thermodynamics of the cell, open circuit voltage (*OCV*) of individual cells was measured in response to different states of charge (*SOC*), while maintaining various temperature differences between the cells. This was necessary so that ΔE value between the cells could be obtained as that potential difference is proportional to the energy that could be used for work due to temperature difference, i.e. conversion of heat to electricity.

Measurements were conducted with two different concentrations of the electrolytes in order to examine if higher concentrations would yield greater potential differences at the same temperature and *SOC* values, i.e. less overall resistance in the cells.

4.2.1.1 0.1M DHAQ-0.2M $\text{K}_4\text{Fe}(\text{CN})_6 \times 3\text{H}_2\text{O}$

As mentioned above, the measurements of *OCV* vs. *SOC* at various temperature differences were conducted:

$$\Delta T = 35^\circ \text{ (with } T_{\text{COLD}} = 10^\circ \text{C, } T_{\text{HOT}} = 45^\circ \text{C),}$$

$$\Delta T = 30^\circ \text{ (with } T_{\text{COLD}} = 25^\circ \text{C, } T_{\text{HOT}} = 55^\circ \text{C),}$$

$$\Delta T = 50^\circ \text{ (with } T_{\text{COLD}} = 25^\circ \text{C, } T_{\text{HOT}} = 75^\circ \text{C).}$$

The results are shown in Figure 26.

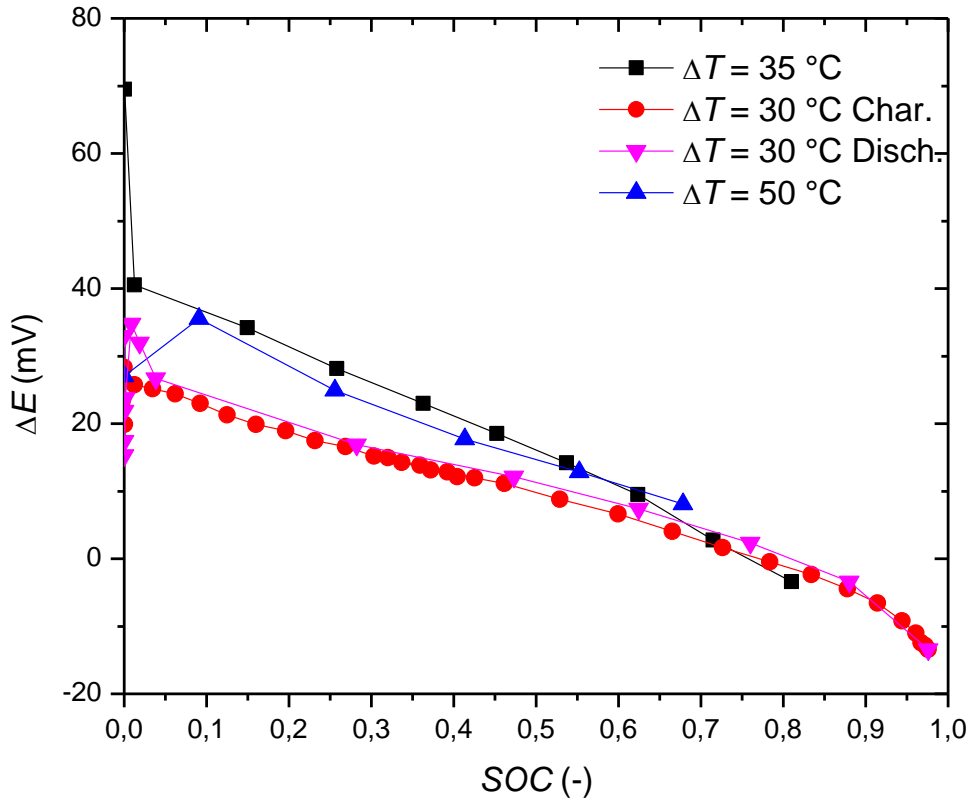


Figure 26. *OCV-SOC* curves for the 0.1 M DHAQ-0.2 M $\text{K}_4\text{Fe}(\text{CN})_6 \times 3\text{H}_2\text{O}$ system with $\Delta T = 35\text{ }^\circ\text{C}$, $\Delta T = 30\text{ }^\circ\text{C}$, $\Delta T = 50\text{ }^\circ\text{C}$

SOC values at different *OCVs* of the cells were determined from a model described in section 3.2.3.1 by inserting different *OCV* values into rearranged Eq. 26 so that it would give out *SOC* values. ΔE values for the cells were calculated as potential difference between hot and cold cell at a given *SOC*. Higher ΔE s were obtained for the measurement with higher ΔT , which is to be expected as it is showed in Eq. 19. that cell potential is proportional to ΔT . However, there are inconsistencies regarding stated conclusions when $\Delta T = 35\text{ }^\circ\text{C}$ measurements are taken into account. It needs to be noted that measurements, since this is only preliminary work, were not done systematically. Due to that, $\Delta T = 35\text{ }^\circ\text{C}$ measurement is not comparable to the rest of the measurements, nevertheless, it is interesting to present the results for the reasons stated later.

Further, as seen from Eq. 19. and 21. potential difference of the cells has an entropy dependence as well as a Nernstian part, i.e. Eq. 21. Above 50% *SOC* values, the Nernst part of the equation in this particular system starts to become dominant and *OCV* values between cells quickly start dropping to zero. For our redox system, around 75% of *SOC*, cell potential has dropped to zero for all measurements, regardless of the ΔT values.

Cells were taken apart after measurements at $\Delta T = 35\text{ }^\circ\text{C}$ (with $T_{\text{COLD}} = 10\text{ }^\circ\text{C}$, $T_{\text{HOT}} = 45\text{ }^\circ\text{C}$), since the system started to clog. Precipitation has been found on the flow pattern of the graphite blocks and on the carbon paper of the cold cell, see Figure 27.



Figure 27. Precipitation in the cold cell at $T_{COLD} = 10\text{ }^{\circ}\text{C}$

Therefore, further measurements with $T_{COLD} = 10\text{ }^{\circ}\text{C}$ were discarded, and the lowest temperature of cold cell at which the measurements were conducted was room temperature, i.e. the temperature at which the solutions were prepared to assure no further precipitation would appear.

4.2.1.2 0.2M DHAQ and 0.4M $\text{K}_4\text{Fe}(\text{CN})_6 \cdot 3\text{H}_2\text{O}$

As mentioned above, various sets of temperature differences were conducted for the higher concentrations of redox pairs:

$$\Delta T = 30^{\circ} \text{ (with } T_{COLD} = 25\text{ }^{\circ}\text{C, } T_{HOT} = 55\text{ }^{\circ}\text{C),}$$

$$\Delta T = 50^{\circ} \text{ (with } T_{COLD} = 25\text{ }^{\circ}\text{C, } T_{HOT} = 75\text{ }^{\circ}\text{C).}$$

The obtained results results are shown in Figure 28.

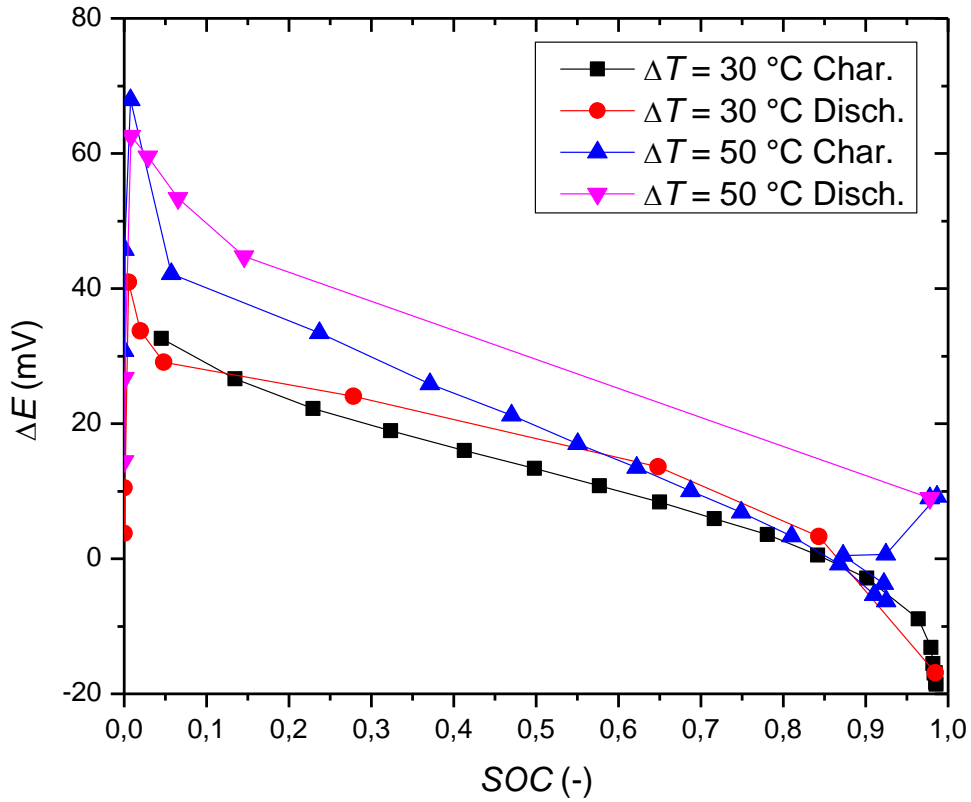


Figure 28. *OCV-SOC* curves for the 0.2 M DHAQ-0.4 M $\text{K}_4\text{Fe}(\text{CN})_6 \times 3\text{H}_2\text{O}$ system with $\Delta T = 30\text{ }^{\circ}\text{C}$, $\Delta T = 50\text{ }^{\circ}\text{C}$

Indeed, there is a greater potential difference at higher concentrations, although, this effect is not significant and it is showing around 5 mV higher ΔE through all of the *SOC* range when compared to lower concentrations. However, it is worth noting all the equipment problems that occurred at this point of tests, specifically with higher concentration measurements. Namely, there was a lot of precipitation that occurred on the cells when higher concentrations were used, see Figure 29. It is possible that the graphite blocks were of lower quality and that electrolyte was diffusing through the porous structure of the block over time due to internal pressures that were created. It is therefore, reasonable to assume that the real concentration was not actually that much higher, and possibly, it eventually even became lower than the concentration in the first set of measurements.

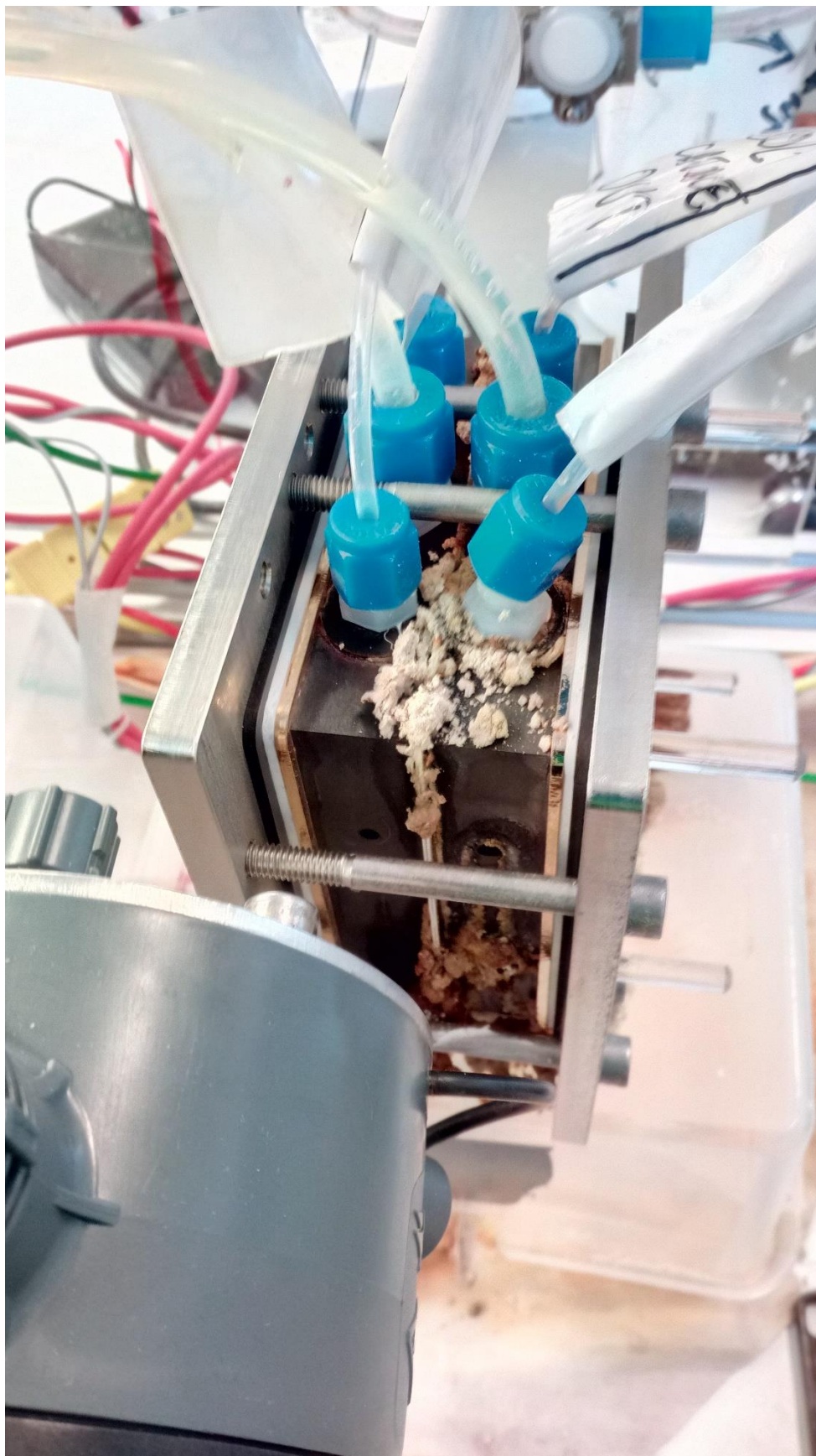


Figure 29. Precipitation that accumulated over time on the cell

It's interesting to notice what happens while the cells are being discharged (at both concentrations). While discharging the cells, relatively big loss in the capacity of the cells can be noticed. Relatively high temperatures at which the cells operate might have a significant impact on battery capacity while current is being drawn thus resulting in big capacity losses. Further, high discharge rates could also significantly lower the amount of energy that could be extracted due to the fact that the redox species do not have enough time for oxidation/reduction reactions to occur properly.

4.2.2 Polarisation measurements

In order to assess heat-battery engine in real life use, it had to be subjected to a load. Therefore, polarisation measurements were conducted while simulating load through charging of hot cell and simultaneously discharging the cold cell with same currents.

E - I polarisation curves of the individual cells were plotted together with the ΔE - I polarisation curves of the system at a given SOC. As previously done, ΔE was calculated by subtracting potential values of the individual cells. The results obtained for 0.1 M DHAQ and 0.2 M $\text{K}_4\text{Fe}(\text{CN})_6 \times 3\text{H}_2\text{O}$ redox system at various states of charge were given in Figure 30. while the results obtained for 0.2 M DHAQ and 0.4 M $\text{K}_4\text{Fe}(\text{CN})_6 \times 3\text{H}_2\text{O}$ redox system at various states of charge were given in Figure 31,32.

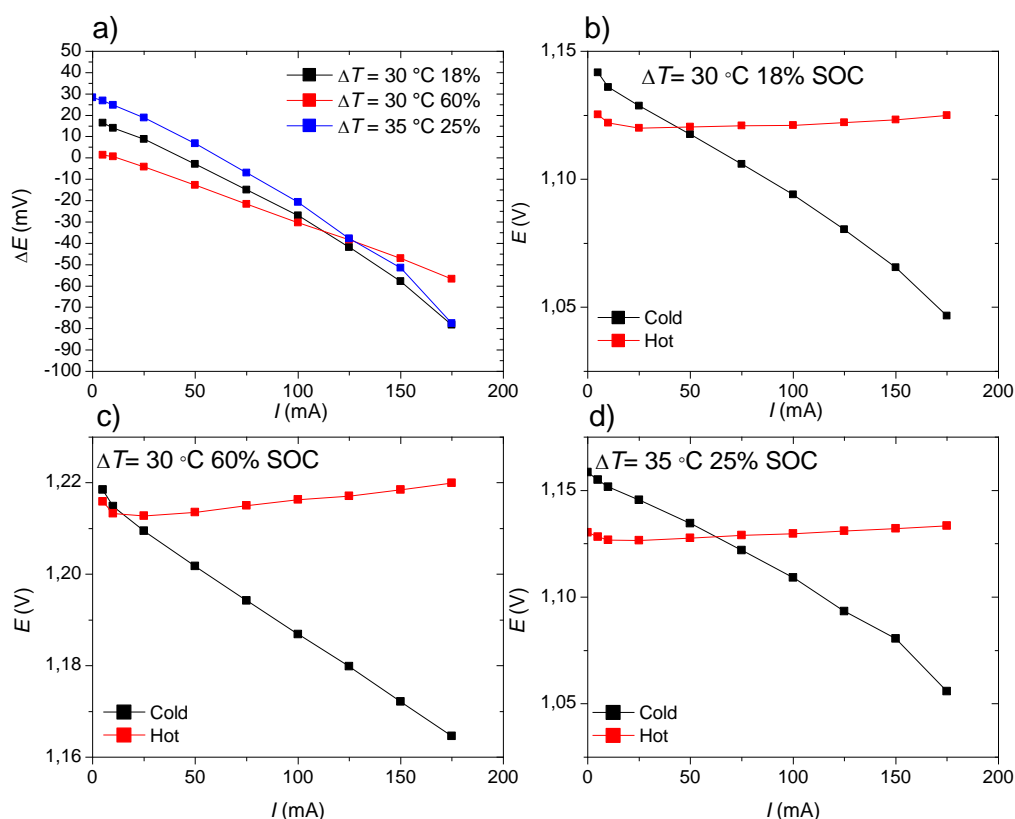


Figure 30. Polarisation curves of the 0.1 M DHAQ and 0.2 M $\text{K}_4\text{Fe}(\text{CN})_6 \times 3\text{H}_2\text{O}$ redox system at various states of charge with: a) ΔE - I polarisation curve at $\Delta T = 30$ °C (SOC at 18 % and 60 %) and $\Delta T = 35$ °C (SOC at 25 %),

b) E - I polarisation curve at $\Delta T = 30\text{ }^{\circ}\text{C}$ (SOC at 18 %), c) E - I polarisation curve at $\Delta T = 30\text{ }^{\circ}\text{C}$ (SOC at 60 %), d) E - I polarisation curve at $\Delta T = 35\text{ }^{\circ}\text{C}$ (SOC at 25 %)

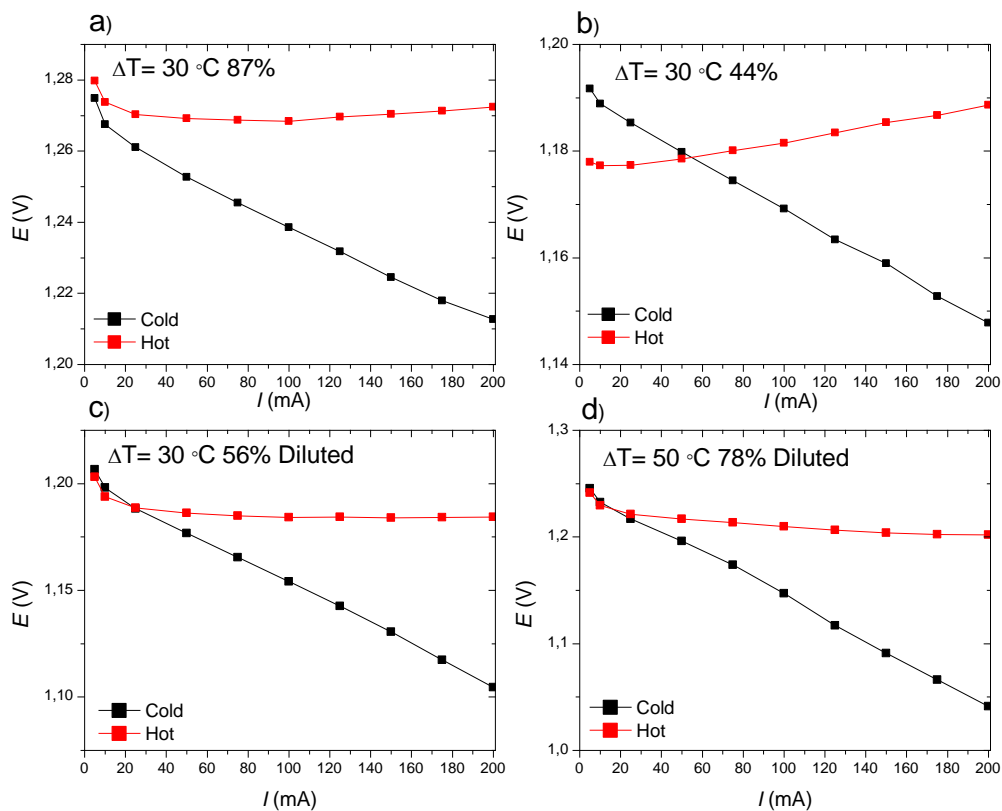


Figure 31. Polarisation curves of the 0.2 M DHAQ and 0.4 M $\text{K}_4\text{Fe}(\text{CN})_6 \cdot 3\text{H}_2\text{O}$ redox system at various states of charge with: a) E - I polarisation curve at $\Delta T = 30\text{ }^{\circ}\text{C}$ (SOC at 87 %), b) E - I polarisation curve at $\Delta T = 30\text{ }^{\circ}\text{C}$ (SOC at 44 %), c) E - I polarisation curve at $\Delta T = 30\text{ }^{\circ}\text{C}$ (SOC at 56 %), d) E - I polarisation curve at $\Delta T = 50\text{ }^{\circ}\text{C}$ (SOC at 78 %)

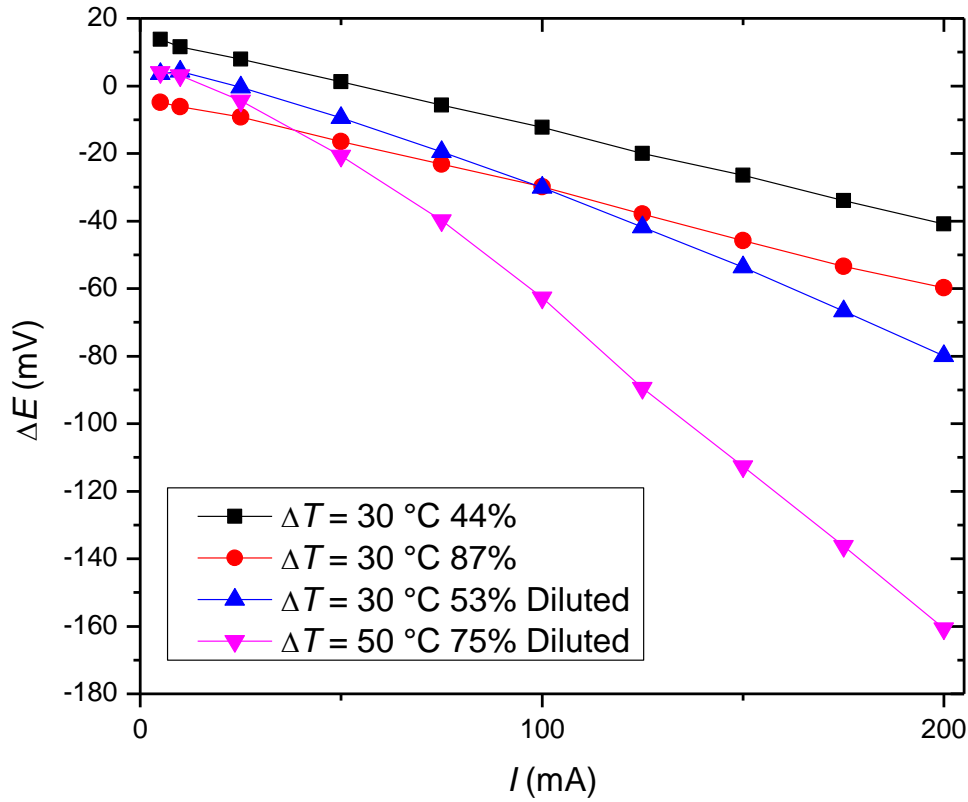


Figure 32. ΔE - I polarisation curves of the system at the $\Delta T = 30$ °C (with $T_{COLD} = 25$ °C and $T_{HOT} = 55$ °C) and $\Delta T = 50$ °C (with $T_{COLD} = 25$ °C and $T_{HOT} = 75$ °C) for the 0.2 M DHAQ and 0.4 M $K_4Fe(CN)_6 \times 3H_2O$ redox system

Analysis of the polarisation results has showed that for the cells with SOC higher than 50%, almost no current could be drawn from the system. If the cells had SOC less than 50%, it was possible to draw currents around 50 mA that could be used for work. However, due to relatively low SOC , OCV values drop to zero quickly, and the highest value was around 60 mV for the system with $\Delta T = 35$ °C, see Figures 30,31,32.

However, once again, it is necessary to take into consideration huge precipitation that occurred for the measurements with higher concentrations, as mentioned in section 4.2.1.2, when interpreting results for higher concentrations.

Further, from the polarisation curves of the individual cells it can be seen that there is a huge potential drop for the cold cells, while the hot cell potential remains around a constant value. Through analysis of linear parts of E - I polarisation curves and with utilization of Ohm's law, see Eq. 33, we are able to get overall resistance of individual cells at different ΔT , see Table 3.

Ohm's law

$$R = \frac{U}{I} \text{ [ohm]} \quad (33)$$

Analysis shows overall cold cell resistance to be around 0.4-0.5 Ω , while the hot cell is exhibiting values of around 0.03-0.04 Ω (see Table 3).

Also, there was clogging of the flow pattern noticed in the cold cell due to carbon paper that degraded inside of the cell, which could be one of the reasons for huge potential drop in cold cell, see Figure 33.

Table 3. Resistances of the individual cells derived from polarisation curves

	$\Delta T / ^\circ\text{C}$	$SOC / \%$	R_{HOT} / Ω	R_{COLD} / Ω
Lower Conc.	35	25	0.014	0.53
	30	18	0.027	0.55
	30	60	0.043	0.23
Higher Conc.	30	44	0.065	0.21
	30	87	0.033	0.26
	30	56	0.024	0.47
	50	78	0.012	1.04

Resistance of the whole system is therefore determined by the cold cell which exhibits resistance of up to 10 times higher than that of the hot cell. Such high resistance is most likely result of the low temperatures, which worsen kinetics of the cells, diffusion of the electrolytes and viscosity as well, thus increasing the potential drop with higher currents. In theory, overall resistance should probably be lowered if the temperatures of the cells were further increased, however, due to internal problems of the cells themselves, such as clogging and precipitation through the graphite blocks, no significant drop in the resistance of the cold cells has been noticed with higher temperature. Other loss mechanisms, such as chemical decomposition of the electrolyte, crossover through the membrane and leakage through the gaskets and from the pumping system, could explain such rapid drops in the potential difference at higher currents as well. *K. Lin at al.* [18] have showed that 2,6, -DHAQ has good stability in alkaline solution in the temperature of up to 100 °C which is well below temperatures examined in this work. However, the stability of ferry/ferrocyanide at higher temperatures is still questionable.

Further, membrane crossover contamination is a common problem in flow batteries. In this alkaline system, however, all the electroactive molecules remain negatively charged in all charge states, leading to significant decrease in possibility of cross-over. Moreover, *K. Lin at al.* [18] have reported, in the alkaline flow battery based on 2,6 – DHAQ and ferry/ferrocyanide electrolytes, low cross-over rates through cation-exchange membranes. Nevertheless, significant discoloration of the electrolytes has been noticed after each test so it is possible that higher temperatures promote cross-over through the membrane even though all of the species are negatively charged. Additionally, each time upon dissembling the cells, coloration was found on the gaskets, indicating the likely site of electrolyte leakage, see Figure 34.

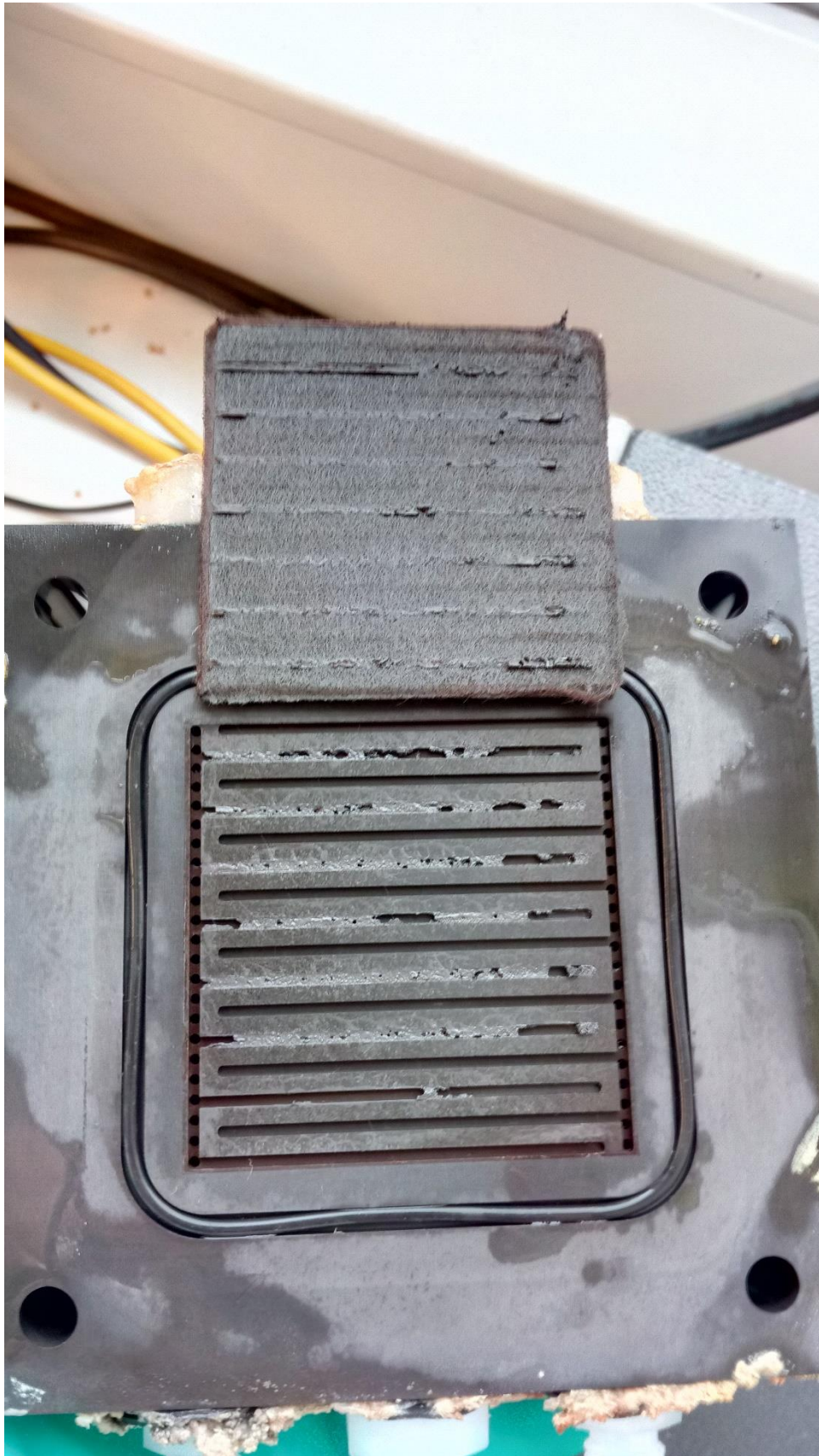


Figure 33. Clogging of the flow pattern with carbon paper

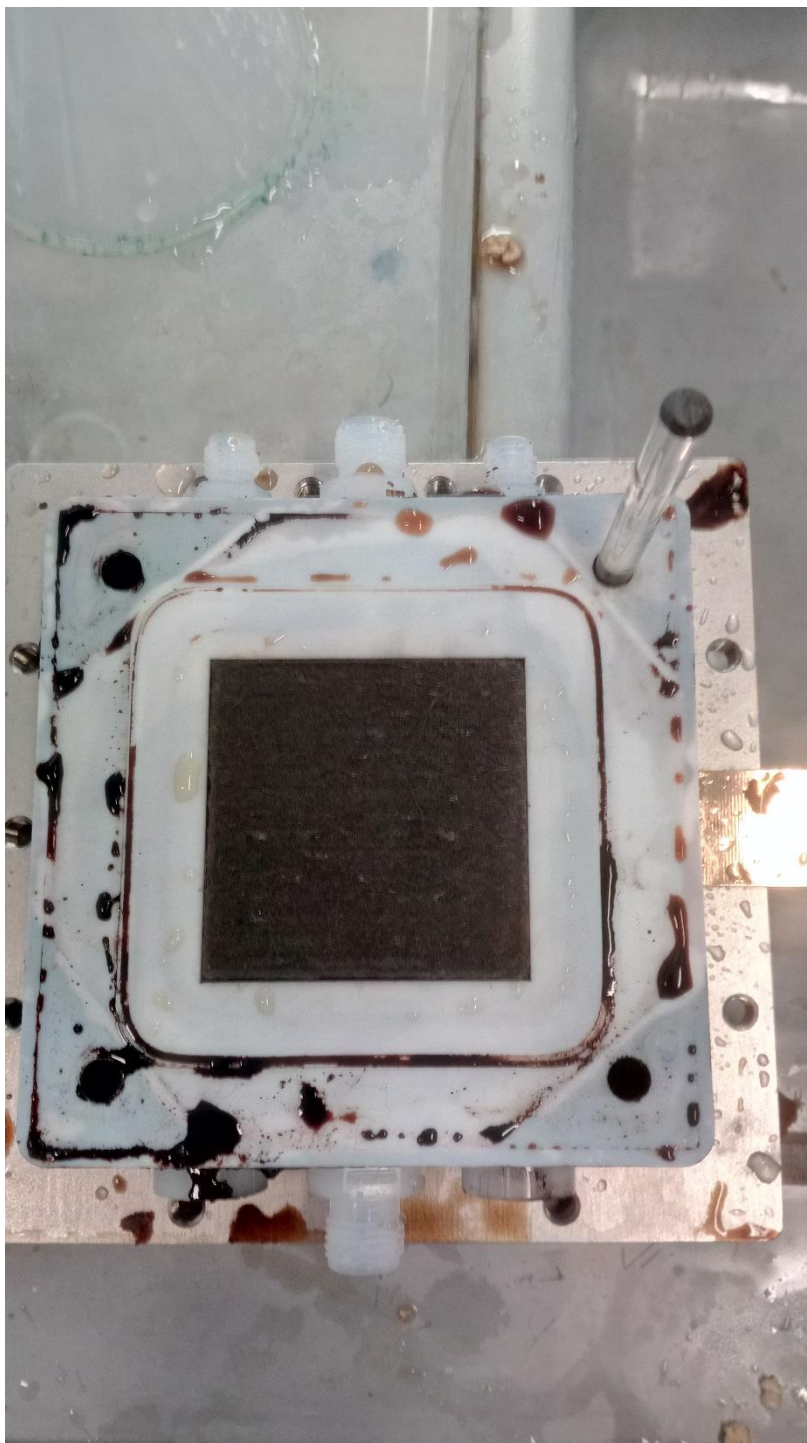


Figure 34. Leakage of electrolyte into gaskets

5 Conclusion

Two cell electrochemical heat engine has been built and this is a proof of concept study that strongly indicates this concept works. With cells active area of 25 cm^2 , around 50 mA could have been extracted out of two cells, i.e. current densities of 2 mA/cm^2 were achieved. Low current densities can be related to the cold cell which exhibited resistance up to ten times higher than that of the hot cell.

For double electrochemical cell heat engines to be commercially competitive, effort should be made in optimization of the cold cell to avoid huge ohmic losses, which could significantly improve current densities.

6 References

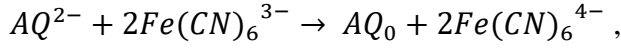
1. Pan F., Wang Q., Redox Species of Redox Flow Batteries: A Review, *Molecules*, **20** (2015) 20499-517.
2. Lee SW., Yang Y., Lee HW, Ghasemi H., Kraemer D., Chen G., Cui Y., An electrochemical system for efficiently harvesting low-grade heat energy, *Nature communications*, (2014) 5-3942.
3. <http://large.stanford.edu/courses/2010/ph240/weisse1/> (accessed 15. September 2017.)
4. Gunawan A., Lin CH, Buttry D. A., Mujica V., Taylor R. A., Prasher R. S., Phelan P. E., Liquid thermoelectric: Review of recent and limited new data of thermogalvanic cell experiments, *Nanoscale and microscale thermophysical engineering*, **17** (2013) 304-323.
5. Agar J.N., Thermogalvanic Cells, in P. Delahay and C.W. Tobias, *Advances in Electrochemistry and Electrochemical Engineering*, New York, Interscience, VOL 3 (1963) 31-121
6. Hu R., Cola B. A., Haram N., Barisci J.N., Lee S., Stoughton S., Wallace G., Too C., Thomas M., Gestos A., Cruz M., Ferraris J. P., Zakhidov A. A., Baughman R. H., Harvesting waste thermal energy using a carbon-nanotube-based thermo-electrochemical cell, *Nano letters*, **10** (2010) 836-846
7. Chalamala B.R., Fisher G.R., Viswanathan V.V., Perry M.L., Redox flow batteries: An engineering perspective, *Proceeding of the IEEE*, **102** (2014) 976-999
8. Alotto P., Guarnieri M., Moro F., Redox flow batteries for the storage of renewable energy: A review, *Renewable and sustainable energy reviews*, **29** (2014) 325-335
9. Mabbott G.A., An introduction to cyclic voltammetry, *Journal of chemical education*, **60** (1983) 697-702
10. Brownson D.A.C., Banks C.E., *The handbook of grapheme electrochemistry*, Springer, London, 2014, 35-43
11. Bratsch S.G., Standard electrode potentials and temperature coefficients in water at 298.15 K, *Journal of physical chemistry*, **18** (1989) 1
12. Ansuini F.J., Diamond J.R., Factors affecting the accuracy of reference electrodes, *Materials performance*, **33** (1994) 14-17
13. Gong S., Lu J., Yan H., Developing the self-contained hydrogen reference electrode, *Journal of electroanalytica chemistry*, **436** (1997) 291-293
14. Inzelt G., Lewenstam A., Scholz F., *Handbook of reference electrodes*, Springer, Berlin, 2013, 331-332
15. Benziger J.B., Satterfiels M.B., Hogarth W.H.J., Nehlsen J.P., Kevrekidis I.G., The power performance curve for engineering analysis of fuel cells, *Journal of power sources*, **155** (2006) 272-285
16. Shindo K., Arakawa M., Hirai T., Influence of electrode materials on open-circuit voltage profile with a temperature difference for a thermocell using a Br^2/Br^- - redox reaction, *Journal of power sources*, **110** (2002) 46-51
17. Gerhardt M.R., Tong L., Gomez-Bombarelli R., Chen Q., Marshak M.P., Galvin C.J., Aspuru-Guzik A., Gordon R.G., Aziz M.J., Anthraquinone derivatives in aqueous flow batteries, *Advanced energy materials*, **7** (2017) 1-9
18. Lin K., Chen Q., Gerhardt M.R., Tong L., Kim S.B. Eisenach L., Valle A.W., Hardee D., Gordon R.G., Aziz M.J., Marshak M.P., Alkaline quinone flow battery, *Science*, **349** (2015) 1529-1532
19. Kasem K.K., Jones S., Platinum as a reference electrode in electrochemical measurements, *Platinum metals review*, **52** (2008) 100-106

20. Østedgaard-Munck D.N., Catalano J. Kristensen M.B., Bentien A., Data on flow cell optimization for membrane based electrokinetic energy conversion, *Materials today energy*, **5** (2017) 118-125
21. Østedgaard-Munck D.N., Catalano J. Kristensen M.B., Bentien A., Membrane-based electrokinetic energy conversion, *Data in brief*, **15** (2017) 1-11

7 Appendix

7.1 A1- Derivation of Q for the tested flow battery system

For equation



$$Q = \frac{[AQ] [Fe(CN)_6^{4-}]^2}{[AQ^{2-}][Fe(CN)_6^{3-}]^2}$$

And

$$SOC = \frac{[AQ^{2-}]}{[AQ]_0},$$

where $[AQ^{2-}] = [AQ]_0 SOC$

$$SOC = 1 - \frac{[AQ]}{[AQ]_0} \rightarrow [AQ] = [AQ]_0(1 - SOC)$$

$$[Fe(CN)_6^{4-}] = 2[AQ]$$

$$[Fe(CN)_6^{3-}] = 2[AQ^{2-}]$$

Therefore,

$$Q = \frac{4[AQ]^3}{4[AQ^{2-}]^3} = \left(\frac{[AQ]_0(1 - SOC)}{[AQ]_0 SOC} \right)^3 = \frac{(1 - SOC)^3}{SOC^3}$$

Curriculum Vitae

First Name & Last name: Marko Plazanić



Education & Training

- **2015 -**
Competing for Master's Degree in Chemical process engineering at the Faculty of chemical engineering and technology, Zagreb; expected graduation: September 2017
- **2012-2015**
Bachelor's degree in Chemical engineering, Faculty of chemical engineering and technology, Zagreb
- **2008-2012**
Highschool graduate, A. G. Matoš highschool, Samobor

Additional information

- **A scientific research "Preparation of self-assembled monolayers of organic acids via electrochemical deposition", Department of electrochemistry (Faculty of chemical engineering and technology, Zagreb)**
- **BEST (Board of European students of technology)
Zagreb Spring Course 2014**
- **14th Croatian festival of science, Zagreb, April 2016**